Hindawi
International Journal of Aerospace Engineering
Volume 2023, Article ID 4692840, 19 pages
https://doi.org/10.1155/2023/4692840

Research Article

Adaptive Distributed Fixed-Time Cooperative Three-Dimensional Guidance Law for Multimissiles against Manoeuvring Target

Jiwei Gao,[1] **Xiaojing Li**,[2] **Shaofei Zang**,[1] **Jianwei Ma**,[1] **and Jinpeng Zhang**[3]

[1]*School of Information Engineering, Henan University of Science and Technology, Luoyang 471023, China*
[2]*Luoyang Institute of Science and Technology, Luoyang 471023, China*
[3]*National Key Laboratory of Air-Based Information Perception and Fusion, Luoyang 471099, China*

Correspondence should be addressed to Jiwei Gao; jwgao2012@163.com

Received 13 July 2023; Revised 8 November 2023; Accepted 27 November 2023; Published 21 December 2023

Academic Editor: Binbin Yan

The problem of cooperative interception of the manoeuvring target is investigated in this paper. Firstly, in light of fast fixed-time consensus theory, time-to-go, and undirected topologies, adaptive cooperative guidance along the line-of-sight (LOS) direction is proposed to guarantee impact time synchronization. Next, novel nonsingular terminal sliding mode (NTSM) is designed to establish adaptive fixed-time guidance law for steering LOS angular rates to the origin or its small neighbourhood. Without the knowledge of target manoeuvre, the proposed cooperative guidance law can be provided by lateral and longitudinal accelerations of each missile, while more reasonable and rigorous analysis of fixed-time stability is carried out through the Lyapunov theory. Within the specified time, both control tasks of simultaneous attack and the desired impact angles can be completed before the final time of the guidance process. Finally, numerical simulations demonstrate the feasibility and effectiveness of the proposed scheme.

1. Introduction

With the development of science and technology in the military field, the importance and significance of multiple missiles jointly intercepting or attacking one target, which can reduce the miss distance and enhance the destruction intensity, have become increasingly prominent. In this field, two important aspects, that is, a group of missiles reaches the target simultaneously and each missile attacks the target with different impact angles, may be generally considered. In [1], distributed cooperative guidance law is proposed to achieve the expected impact angle, while sufficient condition on arbitrary time-varying topologies is established to accomplish impact time consensus. For two-dimensional (2D) and three-dimensional (3D) scenarios of stationary target [2], impact angle-constrained salvo attack is achieved by the proposed cooperative guidance laws. In [3], 3D cooperative guidance of multiple spatial-temporal constraints is accomplished without active speed control. Finite-time observer is constructed to estimate full states and disturbances [4], and then, two parts are, respectively, designed to guarantee that simultaneous hit-to-kill attack can be realized at the desired impact angles. Similarly, individual and cooperative parts are proposed to make all missiles hit target simultaneous from the desired direction [5]. For 3D space attack of stationary target [6], normal accelerations are constructed to make azimuth and elevation LOS angle errors converge to the origin within the specified time, and tangential acceleration is designed to maintain the variables of the time-to-go reaching the consensus.

So far, some methodologies have been applied to this field, and several achievements have been made. In [7], PNG law and impact time error feedback are combined to formulate new guidance scheme such that stationary target can be simultaneously hit by antiship missiles. In the pitch and yaw channels [8], augmented PNG and time-to-go coordination laws are, respectively, designed to solve cooperative guidance problem. With coverage strategy [9], cooperative guidance law is designed to intercept strong manoeuvrable target. In [10], prescribed-time optimal consensus and typical pure PNG law are applied to establish first-stage and second-stage cooperative schemes, respectively, and salvo

attack is finally realized. Similarly, field-of-view two-stage guidance law is designed to achieve salvo attack without time-to-go estimation based on inverse optimal approach and typical pure PNG law [11]. Nonsingular sliding mode guidance is derived by the desired impact time [12], while the analysis of capture capability is obtained with different initial conditions. With impact time and angle constraints [13], time-varying sliding mode (SM) is implemented to develop guidance law for homing missiles hitting stationary or moving target. Adaptive law is adopted to deal with the uncertainty [14], while fixed-time stability of simultaneous arrival can be achieved under partial actuator effectiveness.

Among these methods, finite-time cooperative guidance laws with adaptive law and sliding mode technique have received more attention due to smaller miss distance and better antidisturbance performance. In [15], adaptive law, super twisting, integral sliding mode (ISM), and NTSM are implemented to design finite-time 3D cooperative guidance scheme, and simultaneous attack is completed with impact angle constraints. Finite-time consensus is proposed to ensure that vehicles could arrive at the target simultaneously [16], and target accelerations are observed by extended state observer. In the presence and absence of leader missile, finite-time 2D cooperative guidance laws are proposed based on nonhomogeneous observer, super twisting, and SM technique [17]. With directed topologies and impact angle constraint, 3D cooperative guidance law is established to accomplish simultaneous attack based on integral sliding mode (ISM), super twisting, and geometric homogeneity [18].

Fixed-time guidance laws [14, 19–26], which are evolved from finite-time algorithms [15–18, 27, 28], do not depend on the initial states and have better convergent characteristics, so these schemes have further been studied. With time-delay input [20], adaptive cooperative guidance law is proposed to guarantee that the consensus errors converge to the equilibrium point in fixed-time interval. For impact time errors, leader-follower control law is developed to the consensus [21], and guidance commands are proposed to make the interceptors reach the stationary target with desired impact angles. With regard to 3D manoeuvring target, distributed cooperative protocol is adopted to formulate tangential acceleration [22], while normal acceleration is designed to achieve fixed-time convergence of LOS angle errors by ISM technique. Under constraints of topology switching failure, input amplitude, impact time, and angle [23], fast fixed-time NTSM is developed to design adaptive cooperative guidance laws along and perpendicular to LOS directions. Adaptive supertwisting consensus is developed to ensure that time-to-go variables are steered to the equilibrium point [24], while the expected angle constraint is achieved by NTSM and disturbance observer. One method similar to literature [29] is implemented to construct two-order cooperative control law, and then, guidance laws are developed to guarantee fixed-time stabilization of LOS angles in the elevation and azimuth [25]. Likewise, extended state observer and protocol are united to achieve fixed-time consensus [26], and adaptive fixed-time guidance laws are designed to guarantee that LOS angular rates are nullified in the elevation and azimuth LOS directions. Based on the SM observer of the low-pass filtering [30], fixed-time consensus and NTSM are adopted to realize salvo attack and impact angle constraints, respectively. In the process of coordinated attack, a group of missiles can be regarded as special multiagents, so most cooperative guidance laws are established from consensus protocols [29, 31, 32] and guidance laws of single missile [19, 27].

Inspired by the previous researches, this paper adopts consensus protocol, fast fixed-time stability, adaptive law, ISM, and NTSM to solve the problem of multimissile cooperative interception of manoeuvrable target, and some interesting results have been acquired. Compared with the existing literatures, the main contributions or innovations of this paper are provided as follows.

(1) With respect to [2, 6, 18, 21], target manoeuvrability is not considered, and therefore, these cooperative guidance laws could be only applied to intercept stationary target or moving target with constant velocity. In our manuscript, the proposed scheme not only solves 3D interception problem of manoeuvring target but also has better anti-interference performance and higher guidance accuracy

(2) Compared with finite/fixed-time cooperative methodologies [15–18, 21, 24], the settling time of closed-loop subsystem system is not dependent on the initial states by the presented algorithm. In addition, fast fixed-time convergence has been accomplished, and each missile can quickly complete the mission of time-to-go synchronization and interception angle constraints

(3) Two-order consensus protocols are constructed in [21, 25, 26]. Although time-to-go estimation is avoided, the average velocity is uncertain or unknown, which may have certain limitations on the adaptability of these schemes. Therefore, the designed guidance law possesses wider applicability

The structure of this article is provided as follows. In Section 2, preliminaries and problem formulation of cooperative interception are stated. The main results are obtained in Section 3, where mathematical model of geometric engagement is considered, and adaptive fixed-time cooperative guidance law is derived by rigorous stability proof. Numerical simulation is carried out in Section 4. Section 5 draws some conclusions.

2. Preliminaries

2.1. Fixed-Time Stabilization

Definition 1 (see [33, 34]). Consider differential equation

$$\begin{aligned} \dot{x} &= f(t, x), \\ x(0) &= x_0, \end{aligned} \tag{1}$$

with $x \in \mathfrak{R}^n$. $f : \mathfrak{R}_+ \times \mathfrak{R}^n \longrightarrow \mathfrak{R}^n$ is a nonlinear function, which may be discontinuous. If the solutions of (1) are understood in the sense of Filippov, the origin is supposed to be an equilibrium point of system (1).

Definition 2 (see [35]). The origin of (1) is said to be fixed-time stable if it is globally finite-time stable, and the corresponding settling time $T(x_0)$ is bounded, i.e., $\exists T_{\max} > 0 : T(x_0) \le T_{\max}$, $\forall x_0 \in \mathfrak{R}^n$.

Lemma 3 (see [36]). *Let $z_1, z_2, \cdots, z_n$, $0 < p < 0$, and $q \ge 1$ and the following inequalities $(\sum_{i=1}^n z_i)^p \le \sum_{i=1}^n z_i^p$ and $n^{1-q}(\sum_{i=1}^n z_i)^q \le \sum_{i=1}^n z_i^q$ hold.*

Lemma 4 (see [35, 37]). *If there exists one Lyapunov function $V(x)$ such that $\dot{V}(x) \le -\alpha V(x)^p - \beta V(x)^q + \Delta$ holds, where the parameters satisfy $\alpha > 0$, $\beta > 0$, $0 < p < 1$, $q > 1$, and $\Delta > 0$, then the trajectory of system (1) is globally practical fixed-time stable. The corresponding residual set of the solution is expressed as $\Phi = \{\lim_{t \to T} | V(x) \le \min\{(\Delta/\alpha(1-\lambda))^{1/p}, (\Delta/\beta(1-\lambda))^{1/q}\}\}$ with $0 < \lambda < 1$, and the settling time can be estimated by $T(x_0) \le 1/[\alpha(1-p)] + 1/[\beta(q-1)]$.*

Theorem 5. *Consider continuous Lyapunov functions $V(x(t))$ satisfying $\dot{V}(x(t)) \le -\eta_1 V(x(t)) - \eta_2 V^{(p+2)/2}(x(t))/\tanh V^{1/2}(x(t))$ for system (1) with $\eta_1 > 0$ and $\eta_2 > 0$. Then, system trajectory is fixed-time stable, and the settling time is bounded by $2/p\eta_2 \ln(1 + (\eta_2/\eta_1)) + (2/\eta_1(1-p)) \ln(1 + (\eta_1/\eta_2))$.*

Proof. If $V(x) > 1$ is fulfilled, it can be obtained that $\dot{V}(x(t)) \le -\eta_1 V(x(t)) - \eta_2 V^{(p+2)/2}(x(t))$. When circumstance $V(x) \le 1$ arises, the result can be further simplified as $\dot{V}(x(t)) \le -\eta_1 V(x(t)) - \eta_2 V^{(p+1)/2}(x(t))$. Then, define new variable $y = 1 + \ln V$ for $V(x(t)) > 1$ and $y = V^{(1-p)/2}$ for $V(x(t)) \le 1$. Then, the above differential inequality can be further expressed as

$$\begin{cases} \dot{y} = -\eta_1 e^{p(y-1)/2} - \eta_2, & y > 1, \\ \dot{y} = -\dfrac{1-p}{2}(\eta_1 y + \eta_2), & 0 < y \le 1. \end{cases} \tag{2}$$

From (2), the settling time can be calculated as

$$T_m = \lim_{y(x(0)) \to \infty} \left(\int_1^{y(x(0))} \left(\frac{1}{\eta_1 e^{p(y-1)/2} + \eta_2} \right) \mathrm{d}y + \int_0^1 \left(\frac{2}{(1-p)(\eta_1 y + \eta_2)} \right) \mathrm{d}y \right). \tag{3}$$

Select $z = e^{p(y-1)/2}$, and then, (3) can be rewritten as

$$\begin{aligned} T_m &= \lim_{z(x(0)) \to \infty} \left(\int_1^{z(x(0))} \left(\frac{2}{pz(\eta_1 z + \eta_2)} \right) dz + \int_0^1 \left(\frac{2}{(1-p)(\eta_1 y + \eta_1)} \right) dy \right) \\ &= \lim_{z(x(0)) \to \infty} \frac{2}{p\eta_2} \int_1^{z(x(0))} \left(\frac{1}{z} - \frac{1}{z + \eta_2/\eta_1} \right) \mathrm{d}z \\ &\quad + \frac{2}{\eta_1(1-p)} \ln\left(1 + \frac{\eta_1}{\eta_2}\right) \\ &= \frac{2}{p\eta_2} \ln\left(1 + \frac{\eta_2}{\eta_1}\right) + \frac{2}{\eta_1(1-p)} \ln\left(1 + \frac{\eta_1}{\eta_2}\right). \end{aligned} \tag{4}$$

□

Remark 6. Theorem 5 is inspired by [38], and the unified term can ensure that convergent property in both far and near neighbourhoods of the equilibrium point. However, the convergent rate is furthermore improved through introducing one continuous term for differential system in this manuscript, while the upper bound of the settling time has been also analysed by more rigorous logical proof. Subsequently, it is used to design new NTSM surface, which can be widely applied to various nonlinear systems, and furthermore adaptive law is combined to establish fixed-time guidance law.

2.2. Algebraic Graph. Let n missiles intercept one target together, and information communication between them is expressed as the graph $G(V, E, A)$ in the process of cooperative attack. The graph $G(V, E, A)$ consists of a node $V = \{V_1, V_2, \cdots, V_n\}$, an edge $E \subseteq \{(V_i, V_j) : V_i, V_j \in V\}$, and a weighted adjacency matrix $A = [a_{ij}] \in \mathfrak{R}^{n \times n}$. Vertex V_i represents the ith missile; edge (V_i, V_j) denotes an edge of G; $a_{ij} = a_{ji} = 1$ is defined if the ith missile can communicate with the jth missile (namely, they are adjacent), and zero otherwise. The Laplacian matrix of G is defined as $L = [l_{ij}] \in \mathfrak{R}^{n \times n}$ with $l_{ij} = -a_{ij}$ for $i \ne j$ and $l_{ii} = \sum_{j=1}^n a_{ij}$. In addition, the following assumptions are satisfied for the communication graph G.

Assumption 7. The graph G is connected if there is a communication path that involves all the missiles.

Assumption 8. The graph G is undirected if the ith and jth missiles can get information from each other.

Lemma 9 (see [39]). *Consider Laplacian matrix $L = [l_{ij}]$ of the graph G, and the conclusions can be drawn as follows.*

(1) The matrix L is semipositive definite with only one zero eigenvalue, and the other eigenvalues are positive real numbers if and only if the graph G is unconnected

(2) For undirected graph G, the equation $x^T L x = \sum_{i=1}^n \sum_{j=1}^n a_{ij}(x_j - x_i)^2/2$ holds

Lemma 10 (see [39]). *The algebraic connectivity of undirected graph G is expressed by the second small eigenvalue $\lambda_2(L)$ of the Laplacian matrix L. If undirected graph G is connected, the following inequality can be obtained as follows:*

$$\lambda_2(L) = \min_{\|x\| \ne 0, 1_n^T x = 0} \frac{x^T L x}{\|x\|^2} > 0, \tag{5}$$

where 0 is an eigenvalue of L, and 1_n is the associated eigenvector. If the circumstance $\sum_{i=1}^n x_i = 0 (1_n^T x = 0)$ is fulfilled, the following inequality holds:

$$x^T L x \ge \lambda_2(L) x^T x. \tag{6}$$

2.3. Missile-Target Engagement. To simplify pursuit-situation equations, the following assumptions are given: (i) the missiles and target are point masses; (ii) the seeker and autopilot dynamics of the missiles are fast enough to be neglected; and (iii) the accelerations are bounded and unknown between every missile and target, and each missile (interceptor) can only acquire the corresponding velocities and positions for each other. Under these assumptions, 3D interception geometry is shown in Figure 1, and the kinematic relationship between each missile and the target can be expressed in polar coordinates. T and M denote target and missile, respectively. The subscript i stands for variables related with interceptor i. $Ox_Iy_Iz_I$ is the inertial reference frame; $Mx_Iy_Iz_I$ represent the inertial reference frame whose origin is set at the gravity center of missile i. $Mx_Ly_Lz_L$ is the LOS reference frame. r_i, θ_i, and ϕ_i describe the relative distance and the elevation and azimuth angles between each missile and target, respectively. Then, the three-dimensional equations can be obtained from the classical principles of kinematics and dynamics:

$$\begin{aligned} \ddot{r}_i - r_i\dot{\theta}_i^2 - r_i\dot{\phi}_i^2\cos\theta_i &= a_{Tri} - a_{Mri}, \\ r_i\ddot{\phi}_i\cos\theta_i + 2\dot{r}_i\dot{\phi}_i\cos\theta_i - 2r_i\dot{\theta}_i\dot{\phi}_i\sin\theta_i &= a_{T\phi i} - a_{M\phi i}, \\ r_i\ddot{\theta}_i + 2\dot{r}_i\dot{\theta}_i + r_i\dot{\phi}_i\sin\theta_i\cos\theta_i &= a_{T\theta_i} - a_{M\theta i}, \end{aligned} \tag{7}$$

where $\boldsymbol{a}_{Mi} = [a_{Mri}, a_{M\phi i}, a_{M\theta i}]^{\mathrm{T}}$ and $\boldsymbol{a}_T = [a_{Tr}, a_{T\phi}, a_{T\theta}]^{\mathrm{T}}$ represent the acceleration vectors of the ith missile and the target, respectively.

Remark 11. The transformation matrix between the inertial frame and the LOS frame is expressed as

$$R_{LI}(\theta_{Li}, \phi_{Li}) = \begin{bmatrix} \cos\theta_{Li}\cos\psi_{Li} & \cos\theta_{Li}\sin\psi_{Li} & -\sin\theta_{Li} \\ -\sin\psi_{Li} & \cos\psi_{Li} & 0 \\ \sin\theta_{Li}\cos\psi_{Li} & \sin\theta_{Li}\sin\psi_{Li} & \cos\theta_{Li} \end{bmatrix}. \tag{8}$$

Define the acceleration components a_{Mxi}, a_{Myi}, and a_{Mzi} of the missile in the inertial reference frame. Then, from the transformation matrix R_{LI}, it can be obtained that

$$[a_{Mxi}, a_{Myi}, a_{Mzi}]^{\mathrm{T}} = R_{LI}^{-1}[a_{Mri}, a_{M\phi i}, a_{M\theta i}]^{\mathrm{T}}. \tag{9}$$

Remark 12. When interception collision occurs, relative distance r_i belongs to the actual interval $[r_{\min}, r_{\max}]$, which can be considered as the range of miss distance. Herein, $r_{\min}$ and $r_{\max}$ are bounded positive constants. Due to nonzero size, the relationship (10) may be satisfied during the interception engagement

$$r_0 \le r_i(t) \le r_i(0), \quad r_0 \in [r_{\min}, r_{\max}], \tag{10}$$

with the initial relative distance $r_i(0)$.

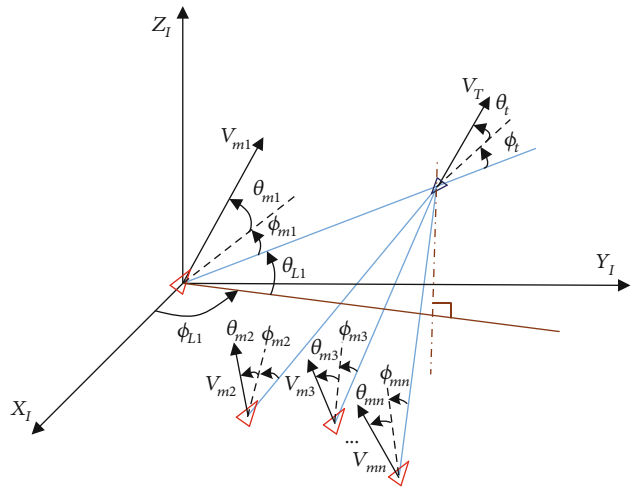

Figure 1: The engagement geometry in 3D space.

3. Main Results

3.1. Tangential Guidance Law Design. Consider expected terminal elevation angle θ_{di} and azimuth angle ϕ_{di} for each missile, which can be selected as the intersect angles or impact angles in three-dimensional engagement scene. At the impact time t_{fi}, the constraint of LOS angles can be expressed as $\theta_{fi} = \theta_{di}$ and $\phi_{fi} = \phi_{di}$. Define new variables x_{ki} $(k = 1, 2, \cdots, 6)$ as $x_{1i} = r_i$, $x_{2i} = \dot{r}_i$, $x_{5i} = \theta_i - \theta_{di}$, $x_{6i} = \dot{\theta}_i$, $x_{3i} = \phi_i - \phi_{di}$, and $x_{4i} = \dot{\phi}_i$. Then, cooperative engagement model can be rewritten as

$$\begin{cases} \dot{x}_{1i} = x_{2i}, \\ \dot{x}_{2i} = x_{1i}x_{6i}^2 + x_{1i}x_{4i}^2\cos\theta_i - a_{Mri} + d_{ri}, \\ \dot{x}_{3i} = x_{4i}, \\ \dot{x}_{4i} = -\dfrac{2x_{2i}x_{4i}}{x_{1i}} + 2x_{4i}x_{6i}\tan\theta_i - \dfrac{a_{M\phi i}}{x_{1i}\cos\theta_i} + d_{\phi i}, \\ \dot{x}_{5i} = x_{6i}, \\ \dot{x}_{6i} = -\dfrac{2x_{2i}x_{6i}}{x_{1i}} - x_{4i}\sin\theta_i\cos\theta_i - \dfrac{a_{M\theta i}}{x_{1i}} + d_{\theta i}, \end{cases} \tag{11}$$

with $d_{ri} = a_{Tri}$, $d_{\phi i} = a_{T\phi i}/(x_{1i}\cos\theta_i)$, and $d_{\theta i} = a_{T\theta i}/x_{1i}$.

Assumption 13. It is assumed that the LOS angles $\theta_i \ne \pm\pi/2$ are fulfilled during the cooperative guidance process.

Firstly, define one variable t_{goi} to denote the time-to-go for each missile interception. Since the relative velocity $\dot{r}_i$ changes slightly in the practical guidance process, t_{goi} can be computed by $t_{goi} = -r_i/\dot{r}_i$. Differentiating t_{goi} versus time yields

$$\dot{t}_{goi} = -1 + \frac{x_{1i}^2x_{6i}^2}{x_{2i}^2} + \frac{x_{1i}^2x_{4i}^2}{x_{2i}^2}\cos\theta_i - \frac{x_{1i}}{x_{2i}^2}a_{Mri} + \frac{x_{1i}}{x_{2i}^2}d_{ri}, \tag{12}$$

Then, introduce another variable t_{fi} to indicate the predictive engagement instant $t_{fi} = t + t_{goi}$, and the derivative of t_{fi} can be expressed as

$$\dot{t}_{fi} = \frac{x_{1i}^2 x_{6i}^2}{x_{2i}^2} + \frac{x_{1i}^2 x_{4i}^2}{x_{2i}^2}\cos\theta_i - \frac{x_{1i}}{x_{2i}^2}a_{Mri} + \frac{x_{1i}}{x_{2i}^2}d_{ri} = \tilde{u}_{ri} + \tilde{d}_{ri}. \tag{13}$$

Therefore, the agreement of t_{fi} is equivalent to that of t_{goi}. If $d_{ri} = 0$ ($\tilde{d}_{ri} = 0$) is fulfilled, the consensus protocol (14) can achieve interception time synchronization for every missile.

Theorem 14. *Consider system (13) ($\tilde{d}_{ri} = 0$) with undirected and connected graph, and the nominal protocol (14) can guarantee that predictive engagement instant t_{fi} realizes fast fixed-time consensus.*

$$\tilde{u}_{ri}^n = \alpha sig\left(\sum_{j\in N_i} a_{ij}\left(t_{fj} - t_{fi}\right)\right)^p + \beta sig\left(\sum_{j\in N_i} a_{ij}\left(t_{fj} - t_{fi}\right)\right)^q + \gamma\sum_{j\in N_i} a_{ij}\left(t_{fj} - t_{fi}\right). \tag{14}$$

Proof. Select the following Lyapunov function:

$$V_1 = \frac{1}{4}\sum_{i=1}^{N}\sum_{j=1}^{N}\alpha_{ij}\left(t_{fj} - t_{fi}\right)^2. \tag{15}$$

Taking the time derivative of (15) yields

$$\begin{aligned}
\dot{V}_1 &= -\sum_{i=1}^{N}\sum_{j=1}^{N} a_{ij}\left(t_{fj} - t_{fi}\right)\cdot\left[\alpha\mathrm{sig}\left(\sum_{j\in N_i} a_{ij}\left(t_{fj} - t_{fi}\right)\right)^p + \beta\mathrm{sig}\left(\sum_{j\in N_i} a_{ij}\left(t_{fj} - t_{fi}\right)\right)^q + \gamma\sum_{j\in N_i} a_{ij}\left(t_{fj} - t_{fi}\right)\right] \\
&= -\alpha\sum_{i=1}^{N}\left|\sum_{j\in N_i} a_{ij}\left(t_{fj} - t_{fi}\right)\right|^{1+p} - \beta\sum_{i=1}^{N}\left|\sum_{j\in N_i} a_{ij}\left(t_{fj} - t_{fi}\right)\right|^{1+q} - \gamma\sum_{i=1}^{N}\left|\sum_{j\in N_i} a_{ij}\left(t_{fj} - t_{fi}\right)\right|^2 \\
&\le -\alpha\left(\sum_{i=1}^{N}\left(\sum_{j=1}^{N} a_{ij}\left(t_{fj} - t_{fi}\right)\right)^2\right)^{1+p/2} - \beta N^{1-q/2}\left(\sum_{i=1}^{N}\left(\sum_{j=1}^{N} a_{ij}\left(t_{fj} - t_{fi}\right)\right)^2\right)^{1+q/2} - \gamma\sum_{i=1}^{N}\left(\sum_{j\in N_i} a_{ij}\left(t_{fj} - t_{fi}\right)\right)^2.
\end{aligned} \tag{16}$$

By Lemma 10, (16) can be furthermore simplified as

$$\dot{V}_1 \le -\alpha\left(2\lambda_2(L_A)V_1\right)^{1+p/2} - \beta N^{1-q/2}\left(2\lambda_2(L_A)V_1\right)^{1+q/2} - \gamma\left(2\lambda_2(L_A)V_1\right). \tag{17}$$

Define another variable $z = V_1^{(1-p)/2}$, and then, differentiating it yields

$$\dot{z} \le -\frac{1-p}{2}\left[\alpha\left(2\lambda_2(L_A)\right)^{1+p/2} + \beta N^{1-q/2}\left(2\lambda_2(L_A)\right)^{1+q/2} z^{q-p/1-p} + 2\gamma\lambda_2(L_A)z\right]. \tag{18}$$

The upper bound of the settling time for (17) or (18) can be estimated by

$$\begin{aligned}
T_1 &\le \int_0^{z(0)} \frac{2}{(1-p)\left[\alpha\left(2\lambda_2(L_A)\right)^{1+p/2} + \beta N^{1-q/2}\left(2\lambda_2(L_A)\right)^{1+q/2} z^{q-p/1-p} + 2\gamma\lambda_2(L_A)z\right]}\mathrm{d}z \\
&= \frac{1}{1-p}\int_1^{z(0)} \frac{1}{\left[2^{p-1/2}\alpha\lambda_2(L_A)^{1+p/2} + 2^{q-1/2}\beta N^{1-q/2}\lambda_2(L_A)^{1+q/2} z^{1+\xi} + \gamma\lambda_2(L_A)z\right]}\mathrm{d}z \\
&\quad + \frac{1}{1-p}\int_0^{1} \frac{1}{\left[2^{p-1/2}\alpha\lambda_2(L_A)^{1+p/2} + 2^{q-1/2}\beta N^{1-q/2}\lambda_2(L_A)^{1+q/2} z^{1+\xi} + \gamma\lambda_2(L_A)z\right]}\mathrm{d}z,
\end{aligned} \tag{19}$$

with $\xi = (q-1)/(1-p)$ and $z(0) = V_1(0)^{1-p/2}$. Furthermore, the following result can be obtained that

$$\begin{aligned}
T_1 &\le \frac{1}{1-p}\left[\int_1^{z(0)} \frac{1}{2^{q-1/2}\beta N^{1-q/2}\lambda_2(L_A)^{1+q/2} z^{1+\xi}}\mathrm{d}z + \int_0^1 \frac{1}{\left[2^{p-1/2}\alpha\lambda_2(L_A)^{1+p/2} + \gamma\lambda_2(L_A)z\right]}\mathrm{d}z\right] \\
&\le \frac{1}{2^{q-1/2}\beta N^{1-q/2}\lambda_2(L_A)^{1+q/2}(q-1)} + \frac{1}{\gamma\lambda_2(L_A)(1-p)}\cdot\ln\left(1 + \frac{\gamma\left(2\lambda_2(L_A)\right)^{1-p/2}}{\alpha}\right).
\end{aligned} \tag{20}$$

This completes the proof. □

Remark 15. Due to relational expression $t_{fj} - t_{fi} = t_{goj} - t_{goi}$, fast fixed-time consensus protocol (14) can be rewritten as

$$\tilde{u}_{ri}^n = \alpha\mathrm{sig}\left(\sum_{j\in N_i} a_{ij}\left(t_{goj} - t_{goi}\right)\right)^p + \beta\mathrm{sig}\left(\sum_{j\in N_i} a_{ij}\left(t_{goj} - t_{goi}\right)\right)^q + \gamma\sum_{j\in N_i} a_{ij}\left(t_{goj} - t_{goi}\right). \tag{21}$$

It can be obtained that this consensus protocol is dependent on information interchange between mutual-communication missiles, and the designed algorithm is one dynamic consensus strategy during guidance process.

In the circumstance $d_{ri} \neq 0$ ($\tilde{d}_{ri} \neq 0$), the nominal consensus protocol cannot guarantee the fixed-time agreement of system (13). According to assumptions (i)-(iii), it can be inferred that the lumped uncertainties $\tilde{d}_{ri}$ is bounded. Therefore, it can be assumed that there exist unknown scalars $\kappa_{ri} > 0$ such that $|\tilde{d}_{ri}| = |x_{1i} d_{ri} / x_{2i}^2| \leq \kappa_{ri} \Theta_{ri}$ holds with $\Theta_{ri} = |x_{1i}/x_{2i}^2|$. Furthermore, consider the following ISM surface:

$$s_{ri} = t_{fi} - t_{fi}(0) - \int_0^t \tilde{u}_{ri}^n dt. \tag{22}$$

By virtue of (22) and parameter adaptation law, robust fixed-time consensus guidance law can be designed as follows:

$$\tilde{u}_{ri} = \tilde{u}_{ri}^n + \tilde{u}_{ri}^c - \eta_1 \mathrm{sig}^{\bar{p}_1}(s_{ri}) - \eta_2 \mathrm{sig}^{\bar{q}_1}(s_{ri}) - \hat{\kappa}_{ri} \Theta_{ri} \ \mathrm{sign}\ (s_{ri}), \tag{23}$$

$$\tilde{u}_{ri}^c = -\frac{s_{ri}}{s_{ri}^2} \frac{c_{1i}(2\varepsilon_{ri} - 1)}{8\varepsilon_{ri}} \left[2^{\bar{p}_1} (1 - \lambda_i) \hat{\kappa}_{ri}^{2\bar{p}_1} + 2^{2\bar{q}_1 - 1} \lambda_i \hat{\kappa}_{ri}^{2\bar{q}_1} \right], \tag{24}$$

$$\dot{\hat{\kappa}}_{ri} = -c_{0i}(c_{1i} \hat{\kappa}_{ri} - \Theta_{ri} |s_{ri}|), \tag{25}$$

where $\varepsilon_{ri} > 0.5$, $0 < \lambda_i < 1$, $\eta_1 > 0$, and $\eta_2 > 0$ are control parameters. c_{0i} and c_{1i} are designed parameters of adaptive law, and $\hat{\kappa}_{ri}$ is estimated value of κ_{ri}.

Theorem 16. *Consider system (13) ($\tilde{d}_{ri} \neq 0$) with undirected and connected graph. The designed guidance law (23)–(25) can ensure that the sliding mode s_i evolves on the manifold and remains there in spite of the uncertainties, and then, fixed-time agreement of t_{goi} can be accomplished.*

Proof. Let us choose the Lyapunov function:

$$V_2 = \frac{1}{2} s_{ri}^2 + \frac{1}{2c_{0i}} (\kappa_{ri} - \hat{\kappa}_{ri})^2. \tag{26}$$

Differentiating (26) yields

$$\begin{aligned} V_2 &= s_{ri} \dot{s}_{ri} + \frac{1}{c_{0i}} (\hat{\kappa}_{ri} - \kappa_{ri}) \dot{\hat{\kappa}}_{ri} \\ &= s_{ri} \left(\tilde{u}_{ri}^c - \eta_1 \mathrm{sig}^{\bar{p}_1}(s_{ri}) - \eta_2 \mathrm{sig}^{\bar{q}_1}(s_{ri}) - \hat{\kappa}_{ri} \Theta_{ri} \ \mathrm{sign}\ (s_{ri}) + \tilde{d}_{ri} \right) \\ &\quad - \frac{1}{c_{0i}} (\kappa_{ri} - \hat{\kappa}_{ri}) \dot{\hat{\kappa}}_{ri}. \end{aligned} \tag{27}$$

By the boundedness inequality of $\tilde{d}_{ri}$ and adaptive updating law (25), one has

$$\begin{aligned} V_2 &\leq s_{ri} \cdot \tilde{u}_{ri}^c - \eta_1 |s_{ri}|^{1+\bar{p}_1} - \eta_2 |s_{ri}|^{1+\bar{q}_1} - \hat{\kappa}_{ri} \Theta_{ri} |s_{ri}| + |s_{ri}| \left| \tilde{d}_{ri} \right| \\ &\quad - \frac{1}{c_{0i}} (\kappa_{ri} - \hat{\kappa}_{ri}) \dot{\hat{\kappa}}_{ri} = s_{ri} \cdot \tilde{u}_{ri}^c - \eta_1 |s_{ri}|^{1+\bar{p}_1} - \eta_2 |s_{ri}|^{1+\bar{q}_1} \\ &\quad + \Theta_{ri} |s_{ri}| (\kappa_{ri} - \hat{\kappa}_{ri}) - \frac{1}{c_{0i}} (\kappa_{ri} - \hat{\kappa}_{ri}) \dot{\hat{\kappa}}_{ri} = s_{ri} \cdot \tilde{u}_{ri}^c - \eta_1 |s_{ri}|^{1+\bar{p}_1} \\ &\quad - \eta_2 |s_{ri}|^{1+\bar{q}_1} + c_{1i} \hat{\kappa}_{ri} (\kappa_{ri} - \hat{\kappa}_{ri}). \end{aligned} \tag{28}$$

Consider the following inequality

$$\hat{\kappa}_{ri} (\kappa_{ri} - \hat{\kappa}_{ri}) \leq \frac{-(2\varepsilon_{ri} - 1)}{2\varepsilon_{ri}} (\kappa_{ri} - \hat{\kappa}_{ri})^2 + \frac{\varepsilon_{ri}}{2} \kappa_{ri}^2, \tag{29}$$

with $\varepsilon_{ri} > 1/2$, and the above result can be further provided as

$$\begin{aligned} V_2 &\leq s_{ri} \cdot \tilde{u}_{ri}^c - \eta_1 |s_{ri}|^{1+\bar{p}_1} - \eta_2 |s_{ri}|^{1+\bar{q}_1} \\ &\quad - \frac{c_{1i}(2\varepsilon_{ri} - 1)}{2\varepsilon_{ri}} (\kappa_{ri} - \hat{\kappa}_{ri})^2 + \frac{\varepsilon_{ri}}{2} \kappa_{ri}^2 \\ &\leq s_{ri} \cdot \tilde{u}_{ri}^c - \eta_1 |s_{ri}|^{1+\bar{p}_1} - \eta_2 |s_{ri}|^{1+\bar{q}_1} \\ &\quad - \frac{c_{1i}(2\varepsilon_{ri} - 1)}{2\varepsilon_{ri}} (1 - \lambda_i) \left(|\kappa_{ri} - \hat{\kappa}_{ri}| - \frac{1}{2} |\kappa_{ri} - \hat{\kappa}_{ri}|^{\bar{p}_1} \right)^2 \\ &\quad - \frac{c_{1i}(2\varepsilon_{ri} - 1)}{2\varepsilon_{ri}} \lambda_i \left(|\kappa_{ri} - \hat{\kappa}_{ri}| - \frac{1}{2} |\kappa_{ri} - \hat{\kappa}_{ri}|^{\bar{q}_1} \right)^2 \\ &\quad - \frac{c_{1i}(2\varepsilon_{ri} - 1)}{2\varepsilon_{ri}} (1 - \lambda_i) |\kappa_{ri} - \hat{\kappa}_{ri}|^{1+\bar{p}_1} \\ &\quad + \frac{1}{4} \frac{c_{1i}(2\varepsilon_{ri} - 1)}{2\varepsilon_{ri}} (1 - \lambda_i) |\kappa_{ri} - \hat{\kappa}_{ri}|^{2\bar{p}_1} \\ &\quad - \frac{c_{1i}(2\varepsilon_{ri} - 1)}{2\varepsilon_{ri}} \lambda_i |\kappa_{ri} - \hat{\kappa}_{ri}|^{1+\bar{q}_1} + \frac{1}{4} \frac{c_{1i}(2\varepsilon_{ri} - 1)}{2\varepsilon_{ri}} \lambda_i |\kappa_{ri} - \hat{\kappa}_{ri}|^{2\bar{q}_1} \\ &\leq s_{ri} \cdot \tilde{u}_{ri}^c - \eta_1 |s_{ri}|^{1+\bar{p}_1} - \eta_2 |s_{ri}|^{1+\bar{\mathrm{q}}_1} \\ &\quad - \frac{c_{1i}(2\varepsilon_{ri} - 1)}{2\varepsilon_{ri}} (1 - \lambda_i) |\kappa_{ri} - \hat{\kappa}_{ri}|^{1+\bar{p}_1} \\ &\quad + \frac{1}{4} \frac{c_{1i}(2\varepsilon_{ri} - 1)}{2\varepsilon_{ri}} (1 - \lambda_i) 2^{\bar{p}_1} \left(\kappa_{ri}^{2\bar{p}_1} + \hat{\kappa}_{ri}^{2\bar{p}_1} \right) \\ &\quad - \frac{c_{1i}(2\varepsilon_{ri} - 1)}{2\varepsilon_{ri}} \lambda_i |\kappa_{ri} - \hat{\kappa}_{ri}|^{1+\bar{q}_1} + \frac{1}{4} \frac{c_{1i}(2\varepsilon_{ri} - 1)}{2\varepsilon_{ri}} \\ &\quad \cdot \lambda_i 2^{2\bar{q}_1 - 1} \left(\kappa_{ri}^{2\bar{q}_1} + \hat{\kappa}_{ri}^{2\bar{q}_1} \right) \leq -\bar{\eta}_1 V_2^{1+\bar{p}_1/2} - \bar{\eta}_2 V_2^{1+\bar{q}_1/2} + \Delta_1, \end{aligned} \tag{30}$$

with $\bar{\eta}_1 = \min\{2^{1+\bar{p}_1/2} \eta_1, (c_{1i}(2\varepsilon_{ri} - 1)/2\varepsilon_{ri})(1 - \lambda_i)(2c_{1i})^{1+\bar{p}_1/2}\}$ and $\Delta_1 = (c_{1i}(2\varepsilon_{ri} - 1)/8\varepsilon_{ri})[2^{\bar{p}_1}(1 - \lambda_i)\kappa_{ri}^{2\bar{p}_1} + 2^{\bar{q}_1} \lambda_i \kappa_{ri}^{2\bar{q}_1}] \bar{\eta}_2 = 2^{1 - \bar{q}_1/2} \min\{2^{1+\bar{q}_1/2} \eta_2, (c_{1i}(2\varepsilon_{ri} - 1)/2\varepsilon_{ri}) \lambda_i (2c_{0i})^{1+\bar{q}_1/2}\}$. According to Lemma 4, it can be inferred that V_2 can converge to the residual of the origin and the setting time T_2 is computed as follows:

$$\begin{aligned} \Phi &= \left\{ \lim_{t \longrightarrow T} \left| V_2 \leq \min \left\{ \left(\frac{\Delta_1}{\bar{\eta}_1 (1 - \vartheta_i)} \right)^{2/1+\bar{p}_1}, \left(\frac{\Delta_1}{\bar{\eta}_2 (1 - \vartheta_i)} \right)^{2/1+\bar{q}_1} \right\} \right\}, \\ T_2 &= \frac{2}{\bar{\eta}_1 \vartheta_i (1 - \bar{p}_1)} + \frac{2}{\bar{\eta}_2 \vartheta_i (\bar{q}_1 - 1)}, \end{aligned} \tag{31}$$

with the constant $0 < \vartheta_i < 1$. Therefore, combined with Theorem 5 and ISM (22), it can be obtained that system is fixed-time stable, and the upper bound of the convergent time is $\bar{T}_1 = T_2 + T_1$. □

Remark 17. In order to avoid chattering of sliding mode manifolds, the sign function in the control can be replaced by some types of approximate continuous function: (1) $f_1(s_i) = s_i/(|s_i| + \hbar_i)$, where $\hbar_i > 0$ is constant and selected to be sufficiently small, and (2) a hyperbolic tangent function $f_2(s_i) = (1 - \exp(-\hbar_i^* s_i))/(1 - \exp(-\hbar_i^* s_i))$ $(\hbar_i^* > 0,\ i = 1, 2, 3)$.

3.2. Normal Guidance Law Design. In this subsection, adaptive guidance law is constructed to guarantee that all the LOS angles of the missiles converge to the desired values without the information on target manoeuvring. Firstly, consider the subsystem for LOS angular rate and angle of azimuth direction:

$$\begin{cases} \dot{x}_{3i} = x_{4i}, \\ \dot{x}_{4i} = -\dfrac{2x_{2i}x_{4i}}{x_{1i}} + 2x_{4i}x_{6i}\tan\theta_i - \dfrac{a_{M\phi i}}{x_{1i}\cos\theta_i} + d_{\phi i}. \end{cases} \tag{32}$$

According to assumptions (i)-(iii) and the characteristics of trigonometric functions, it can be obtained that the perturbations $d_{\phi i}$ are bounded. Therefore, it can be supposed that there exist unknown scalars $\kappa_{\phi i} > 0$ such that $|d_{\phi i}| = |a_{T\phi i}/(x_{1i}\cos\theta_i)| \le \kappa_{\phi i}\Theta_{\phi i}$ is fulfilled with $\Theta_{\phi i} = 1/(x_{1i}\cos\theta_i)$. For accomplishing guidance task for each missile, novel fixed-time SM surface is formulated as follows:

$$s_{\phi i} = x_{4i} + \iota_{11}x_{3i} + \iota_{12}g_{\phi i}(x_{3i}), \tag{33}$$

$$g_{\phi i}(x_{3i}) = \begin{cases} \dfrac{|x_{3i}|^{p'+1}}{\tanh x_{3i}}, & \text{if } \bar{s}_{\phi i} = 0 \,\|\, (\bar{s}_{\phi i} \ne 0 \&\& |x_{3i}| > \varepsilon_\phi), \\ k_{11}x_{3i} + k_{12}\mathrm{sig}^2(x_{3i}), & \text{else } \bar{s}_{\phi i} \ne 0 \&\& |x_{3i}| \le \varepsilon_\phi, \end{cases} \tag{34}$$

$$\bar{s}_{\phi i} = x_{4i} + \iota_{11}x_{3i} + \iota_{12}\frac{|x_{3i}|^{p'+1}}{\tanh x_{3i}}, \tag{35}$$

with $\iota_{11} > 0$, $\iota_{12} > 0$, $k_{11} = (1 - p')\varepsilon_\phi^{p'}/\tanh\varepsilon_\phi$, $k_{12} = p'\varepsilon_\phi^{p'-1}/\tanh\varepsilon_\phi$, and small positive constant ε_ϕ.

Theorem 18. *Consider guidance subsystem (32) for (33) satisfying $s_{\phi i} = \bar{s}_{\phi i} = 0$, and system states can converge to the origin within the specified time $T_{s\phi i} = 1/p'\iota_{12}\ln(1 + (\iota_{12}/\iota_{11})) + (1/(\iota_{11}(1 - p')))\ln(1 + (\iota_{11}/\iota_{12}))$.*

Proof. If the sliding motion occurs, then $s_{\phi i} = \bar{s}_{\phi i} = 0$ is kept on the sliding mode surface. Select another Lyapunov function $V_{s\phi i} = x_{3i}^2$, and its derivative can be written as $\dot{V}_{s\phi i} = -2\iota_{11}x_{3i}^2 - 2\iota_{12}\mathrm{sig}^{p'+2}(x_{3i})/\tanh x_{3i}$. The remaining proof is omitted, which is similar to Lemma 9.

By virtue of these analyses, fixed-time guidance law is proposed as

$$a_{M\phi i} = x_{1i}\cos\theta_i \cdot \left(a_{n\phi i} + k_{\phi 1}\mathrm{sig}^{\bar{p}_2}(s_{\phi i}) + k_{\phi 2}\mathrm{sig}^{\bar{q}_2}(s_{\phi i}) + \frac{\widehat{\kappa}_{\phi i}^*\Theta_{\phi i}^* s_{\phi i}}{2\bar{\omega}_i^2}\right), \tag{36}$$

$$a_{n\phi i} = -\frac{2x_{2i}x_{4i}}{x_{1i}} + 2x_{4i}x_{6i}\tan\theta_i + \iota_{11}x_{4i} + \iota_{12}\dot{g}_{\phi i}(x_{3i}), \tag{37}$$

$$\dot{\widehat{\kappa}}_{\phi i}^* = \gamma_{1i}\left(\frac{\Theta_{\phi i}^* s_{\phi i}^2}{2\bar{\omega}_i^2} - \gamma_{2i}\widehat{\kappa}_{\phi i}^*\right), \tag{38}$$

where positive constants $k_{\phi 1}$, $k_{\phi 2}$, γ_{1i}, and γ_{2i} are the selected parameters. $\widehat{\kappa}_{\phi i}^*$ is the estimation of $\kappa_{\phi i}^2$; $\Theta_{\phi i}^*$ is implemented to denote $\Theta_{\phi i}^2$; the constant $\bar{\omega}_i > 0$ is satisfied. □

Theorem 19. *Consider subsystem (32) with sliding mode surface (33), and adaptive fixed-time guidance law (36)–(38) can guarantee that LOS angular rates and angle errors converge to small regions around the origin within the specified time.*

Proof. Choose the following Lyapunov function:

$$V_3 = \frac{1}{2}s_{\phi i}^2 + \frac{1}{2\gamma_{1i}}\left(\kappa_{\phi i}^* - \widehat{\kappa}_{\phi i}^*\right)^2. \tag{39}$$

The time derivative of V_3 is

$$\begin{aligned} \dot{V}_3 &= s_{\phi i}\dot{s}_{\phi i} - \frac{1}{\gamma_{1i}}\left(\kappa_{\phi i}^* - \widehat{\kappa}_{\phi i}^*\right)\dot{\widehat{\kappa}}_{\phi i}^* \\ &= s_{\phi i}\left[-\frac{2x_{2i}x_{4i}}{x_{1i}} + 2x_{4i}x_{6i}\tan\theta_i - \frac{a_{M\phi i}}{x_{1i}\cos\theta_i} + d_{\phi i} + \iota_{11}x_{4i} + \iota_{12}\dot{g}_{\phi i}(x_{3i})\right] \\ &\quad - \left(\kappa_{\phi i}^* - \widehat{\kappa}_{\phi i}^*\right)\left(\frac{\Theta_{\phi i}^* s_{\phi i}^2}{2\bar{\omega}_i^2} - \gamma_{2i}\widehat{\kappa}_{\phi i}^*\right) \\ &= s_{\phi i}\left[-k_{\phi 1}\mathrm{sig}^{\bar{p}_2}(s_{\phi i}) - k_{\phi 2}\mathrm{sig}^{\bar{q}_2}(s_{\phi i}) - \frac{\widehat{\kappa}_{\phi i}^*\Theta_{\phi i}^* s_{\phi i}}{2\bar{\omega}_i^2} + d_{\phi i}\right] \\ &\quad - \left(\kappa_{\phi i}^* - \widehat{\kappa}_{\phi i}^*\right)\left(\frac{\Theta_{\phi i}^* s_{\phi i}^2}{2\bar{\omega}_i^2} - \gamma_{2i}\widehat{\kappa}_{\phi i}^*\right) \\ &\le -k_{\phi 1}|s_{\phi i}|^{1+\bar{p}_2} - k_{\phi 2}|s_{\phi i}|^{1+\bar{q}_2} - \frac{\widehat{\kappa}_{\phi i}^*\Theta_{\phi i}^* s_{\phi i}^2}{2\bar{\omega}_i^2} + |s_{\phi i}|\kappa_{\phi i}\Theta_{\phi i} \\ &\quad - \frac{\Theta_{\phi i}^* s_{\phi i}^2}{2\bar{\omega}_i^2}\left(\kappa_{\phi i}^* - \widehat{\kappa}_{\phi i}^*\right) + \gamma_{2i}\widehat{\kappa}_{\phi i}^*\left(\kappa_{\phi i}^* - \widehat{\kappa}_{\phi i}^*\right). \end{aligned} \tag{40}$$

Due to the inequality $|s_{\phi i}|\kappa_{\phi i}\Theta_{\phi i} \le (\kappa_{\phi i}^*\Theta_{\phi i}^* s_{\phi i}^2/2\bar{\omega}_i^2) + (\bar{\omega}_i^2/2)$ and (29), the above result can be further derived as

$$\dot{V}_3 \le -\min\left\{k_{\phi 1}, k_{\phi 2}\right\} \cdot \left|s_{\phi i}\right|^2 - \frac{\widehat{\kappa}^*_{\phi i}\Theta^*_{\phi i}s^2_{\phi i}}{2\varpi_i^2} - \frac{\Theta^*_{\phi i}s^2_{\phi i}}{2\varpi_i^2}\left(\kappa^*_{\phi i} - \widehat{\kappa}^*_{\phi i}\right) + \frac{\kappa^*_{\phi i}\Theta^*_{\phi i}s^2_{\phi i}}{2\varpi_i^2} + \frac{\varpi_i^2}{2} - \frac{\left(2\varepsilon_{\phi i}-1\right)}{2\varepsilon_{\phi i}}\left(\kappa^*_{\phi i} - \widehat{\kappa}^*_{\phi i}\right)^2 + \frac{\varepsilon_{\phi i}\left(\kappa^*_{\phi i}\right)^2}{2} \le -\tilde{k}_1 V_3 + \Delta_3, \tag{41}$$

with $\varepsilon_{\phi i} > 1/2$, $\tilde{k}_1 = \min\left\{k_{\phi 1}, k_{\phi 2}, (2\varepsilon_{\phi i}-1)/2\varepsilon_{\phi i}\right\}$, and $\Delta_3 = (\varpi_i^2/2) + (\varepsilon_{\phi i}(\kappa^*_{\phi i})^2/2)$. On the basis of the boundedness theorem, it can be concluded that $s_{\phi i}$ and $\kappa^*_{\phi i} - \widehat{\kappa}^*_{\phi i}$ are uniformly ultimately bounded (UUB). It can be assumed that $|\kappa^*_{\phi i} - \widehat{\kappa}^*_{\phi i}| \le \delta_{\kappa\phi i}$ is fulfilled, where $\delta_{\kappa\phi i}$ are positive constants.

According to the above analysis and inference, the formula (40) can also be converted to the following form:

$$\dot{V}_3 \le -k_{\phi 1}\left|s_{\phi i}\right|^{1+\bar{p}_2} - k_{\phi 2}\left|s_{\phi i}\right|^{1+\bar{q}_2} - \frac{\left(2\varepsilon_{\phi i}-1\right)}{2\varepsilon_{\phi i}}\left(\kappa^*_{\phi i} - \widehat{\kappa}^*_{\phi i}\right)^2 + \frac{\varepsilon_{\phi i}\left(\kappa^*_{\phi i}\right)^2}{2} + \frac{\varpi_i^2}{2} \le -k_{\phi 1}\left(s^2_{\phi i}\right)^{1+\bar{p}_2/2} - k_{\phi 2}\left(s^2_{\phi i}\right)^{1+\bar{q}_2/2} - \left[\frac{\left(2\varepsilon_{\phi i}-1\right)}{2\varepsilon_{\phi i}}\lambda_{\phi i}\left(\kappa^*_{\phi i} - \widehat{\kappa}^*_{\phi i}\right)^2\right]^{1+\bar{p}_2/2} - \left[\frac{\left(2\varepsilon_{\phi i}-1\right)}{2\varepsilon_{\phi i}}\left(1-\lambda_{\phi i}\right)\left(\kappa^*_{\phi i} - \widehat{\kappa}^*_{\phi i}\right)^2\right]^{1+\bar{q}_2/2} + \widehat{\Delta}_3, \tag{42}$$

with $\widehat{\Delta}_3 = \left[\left((2\varepsilon_{\phi i}-1)/2\varepsilon_{\phi i}\right)\lambda_{\phi i}(\kappa^*_{\phi i} - \widehat{\kappa}^*_{\phi i})^2\right]^{1+\bar{p}_2/2} + \left[\left((2\varepsilon_{\phi i}-1)/2\varepsilon_{\phi i}\right)(1-\lambda_{\phi i})(\kappa^*_{\phi i} - \widehat{\kappa}^*_{\phi i})^2\right]^{1+\bar{q}_2/2} - \left((2\varepsilon_{\phi i}-1)/2\varepsilon_{\phi i}\right)(\kappa^*_{\phi i} - \widehat{\kappa}^*_{\phi i})^2 + (\varepsilon_{\phi i}(\kappa^*_{\phi i})^2/2) + (\varpi_i^2/2)$ and $1/2 < \lambda_{\phi i} < 1$. Now, further analysis for $\widehat{\Delta}_3$ will be carried out. Consider the circumstance $\lambda_{\phi i}(2\varepsilon_{\phi i}-1)(\kappa^*_{\phi i} - \widehat{\kappa}^*_{\phi i})^2/(2\varepsilon_{\phi i}) \le 1$, and then, one has

$$\left[\frac{\left(2\varepsilon_{\phi i}-1\right)}{2\varepsilon_{\phi i}}\lambda_{\phi i}\left(\kappa^*_{\phi i} - \widehat{\kappa}^*_{\phi i}\right)^2\right]^{1+\bar{p}_2/2} + \left[\frac{\left(2\varepsilon_{\phi i}-1\right)}{2\varepsilon_{\phi i}}\left(1-\lambda_{\phi i}\right)\left(\kappa^*_{\phi i} - \widehat{\kappa}^*_{\phi i}\right)^2\right]^{1+\bar{q}_2/2} - \frac{\left(2\varepsilon_{\phi i}-1\right)}{2\varepsilon_{\phi i}}\left(\kappa^*_{\phi i} - \widehat{\kappa}^*_{\phi i}\right)^2 \le \left[\frac{\left(2\varepsilon_{\phi i}-1\right)}{2\varepsilon_{\phi i}}\lambda_{\phi i}\left(\kappa^*_{\phi i} - \widehat{\kappa}^*_{\phi i}\right)^2\right]^{1+\bar{p}_2/2} - \frac{\left(2\varepsilon_{\phi i}-1\right)}{2\varepsilon_{\phi i}}\lambda_{\phi i}\left(\kappa^*_{\phi i} - \widehat{\kappa}^*_{\phi i}\right)^2 < 1. \tag{43}$$

When the case $\lambda_{\phi i}(2\varepsilon_{\phi i}-1)(\kappa^*_{\phi i} - \widehat{\kappa}^*_{\phi i})^2/(2\varepsilon_{\phi i}) > 1 \ge (1-\lambda_{\phi i})(2\varepsilon_{\phi i}-1)(\kappa^*_{\phi i} - \widehat{\kappa}^*_{\phi i})^2/(2\varepsilon_{\phi i})$ appears, it has

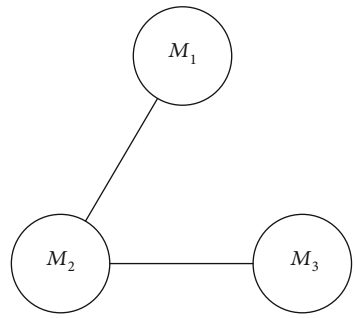

Figure 2: Communication topology among the missiles.

Table 1: The initial conditions of the missiles.

M_i	$r(0)$	$\dot{r}(0)$	$\phi(0)$	$\dot{\phi}(0)$	$\theta(0)$	$\dot{\theta}(0)$
M_1	10000	-417.57	$\pi/6$	-0.0056	$\pi/6$	-0.0028
M_2	9491.63	-380.35	0.5408	-0.0141	1.1491	-0.0059
M_3	9587.51	-409.80	0.3733	-0.0107	1.1274	-0.0046

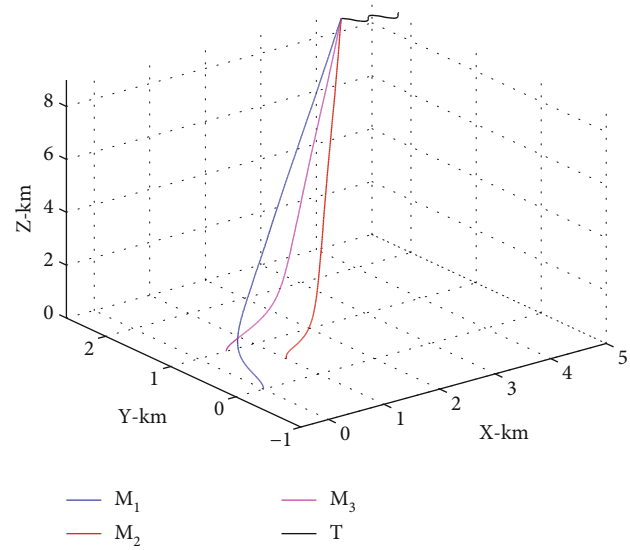

Figure 3: The engagement trajectories under the proposed scheme.

$$\left[\frac{\left(2\varepsilon_{\phi i}-1\right)}{2\varepsilon_{\phi i}}\lambda_{\phi i}\left(\kappa^*_{\phi i} - \widehat{\kappa}^*_{\phi i}\right)^2\right]^{1+\bar{p}_2/2} + \left[\frac{\left(2\varepsilon_{\phi i}-1\right)}{2\varepsilon_{\phi i}}\left(1-\lambda_{\phi i}\right)\left(\kappa^*_{\phi i} - \widehat{\kappa}^*_{\phi i}\right)^2\right]^{1+\bar{q}_2/2} - \frac{\left(2\varepsilon_{\phi i}-1\right)}{2\varepsilon_{\phi i}}\left(\kappa^*_{\phi i} - \widehat{\kappa}^*_{\phi i}\right)^2 \le 0. \tag{44}$$

If the condition $\lambda_{\phi i}(2\varepsilon_{\phi i}-1)(\kappa^*_{\phi i} - \widehat{\kappa}^*_{\phi i})^2/(2\varepsilon_{\phi i}) \ge (1-\lambda_{\phi i})(2\varepsilon_{\phi i}-1)(\kappa^*_{\phi i} - \widehat{\kappa}^*_{\phi i})^2/(2\varepsilon_{\phi i}) > 1$ is satisfied, it follows

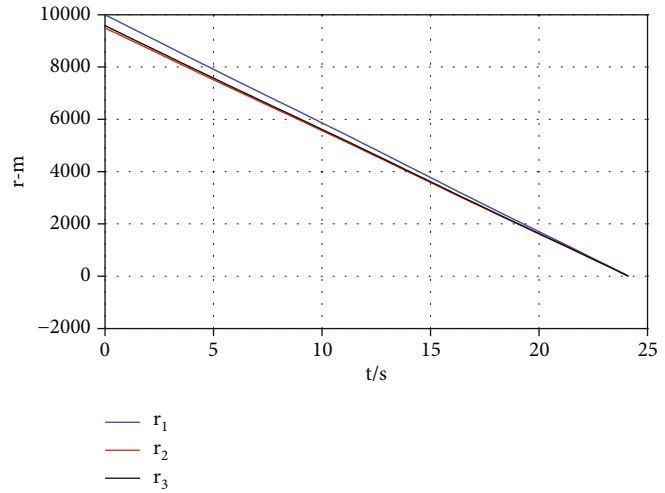

Figure 4: Relative distances under the proposed scheme.

$$\begin{aligned}
&\left[\frac{(2\varepsilon_{\phi i}-1)}{2\varepsilon_{\phi i}}\lambda_{\phi i}\left(\kappa_{\phi i}^{*}-\widehat{\kappa}_{\phi i}^{*}\right)^{2}\right]^{1+\bar{p}_{2}/2}\\
&\quad+\left[\frac{(2\varepsilon_{\phi i}-1)}{2\varepsilon_{\phi i}}(1-\lambda_{\phi i})\left(\kappa_{\phi i}^{*}-\widehat{\kappa}_{\phi i}^{*}\right)^{2}\right]^{1+\bar{q}_{2}/2}\\
&\quad-\frac{(2\varepsilon_{\phi i}-1)}{2\varepsilon_{\phi i}}\left(\kappa_{\phi i}^{*}-\widehat{\kappa}_{\phi i}^{*}\right)^{2}\\
&\le\left[\frac{(2\varepsilon_{\phi i}-1)}{2\varepsilon_{\phi i}}(1-\lambda_{\phi i})\left(\kappa_{\phi i}^{*}-\widehat{\kappa}_{\phi i}^{*}\right)^{2}\right]^{1+\bar{q}_{2}/2}\\
&\quad-\frac{(2\varepsilon_{\phi i}-1)}{2\varepsilon_{\phi i}}(1-\lambda_{\phi i})\left(\kappa_{\phi i}^{*}-\widehat{\kappa}_{\phi i}^{*}\right)^{2}.
\end{aligned}\tag{45}$$

From UUB analysis of adaptive parameter $\widehat{\kappa}_{\phi i}^{*}$, the above results can be summarized as

$$\begin{aligned}
&\left[\frac{(2\varepsilon_{\phi i}-1)}{2\varepsilon_{\phi i}}\lambda_{\phi i}\left(\kappa_{\phi i}^{*}-\widehat{\kappa}_{\phi i}^{*}\right)^{2}\right]^{1+\bar{p}_{2}/2}\\
&\quad+\left[\frac{(2\varepsilon_{\phi i}-1)}{2\varepsilon_{\phi i}}(1-\lambda_{\phi i})\left(\kappa_{\phi i}^{*}-\widehat{\kappa}_{\phi i}^{*}\right)^{2}\right]^{1+\bar{q}_{2}/2}-\frac{(2\varepsilon_{\phi i}-1)}{2\varepsilon_{\phi i}}\left(\kappa_{\phi i}^{*}-\widehat{\kappa}_{\phi i}^{*}\right)^{2}\\
&\le\max\left\{1,\left[\frac{(2\varepsilon_{\phi i}-1)}{2\varepsilon_{\phi i}}(1-\lambda_{\phi i})\delta_{\kappa\phi i}^{2}\right]^{1+\bar{q}_{2}/2}-1\right\}
\end{aligned}\tag{46}$$

Then, the inequality (42) can be furthermore expressed as

$$\dot{V}_{3}\le-\bar{k}_{1}V_{3}^{1+\bar{p}_{2}/2}-\bar{k}_{1}V_{3}^{1+\bar{q}_{2}/2}+\bar{\Delta}_{3},\tag{47}$$

with $\bar{k}_{1}=\min\{2^{1+\bar{p}_{2}/2}k_{\phi 1},[(2\varepsilon_{\phi i}-1)\lambda_{\phi i}\gamma_{1i}/\varepsilon_{\phi i}]^{1+\bar{p}_{2}/2}\}$, $\bar{k}_{2}=\min\{2k_{\phi 2},2^{1-\bar{q}_{2}/2}[(2\varepsilon_{\phi i}-1)(1-\lambda_{\phi i})\gamma_{1i}/\varepsilon_{\phi i}]^{1+\bar{q}_{2}/2}\}$, and $\bar{\Delta}_{3}=\max\{1,[((2\varepsilon_{\phi i}-1)/2\varepsilon_{\phi i})(1-\lambda_{\phi i})\delta_{\kappa\phi i}^{2}]^{1+\bar{q}_{2}/2}-1\}+(\varepsilon_{\phi i}(\kappa_{\phi i}^{*})^{2}/2)+(\varpi_{i}^{2}/2)$.

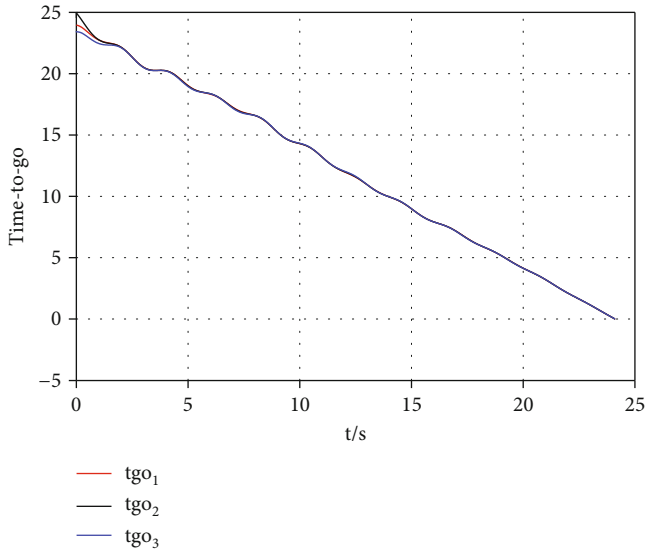

Figure 5: Time-to-go under the proposed scheme.

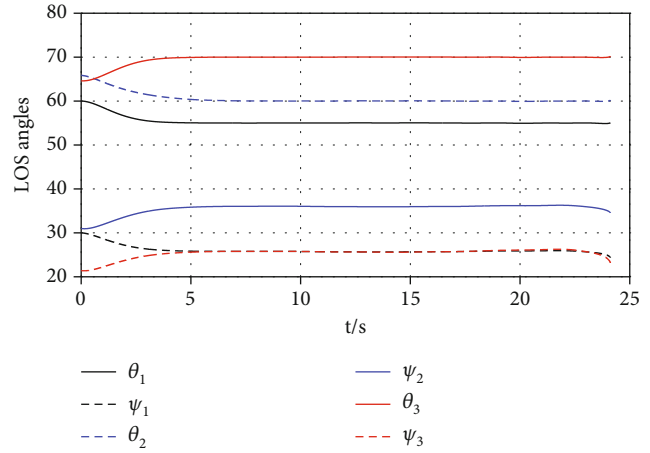

Figure 6: LOS angles under the proposed scheme.

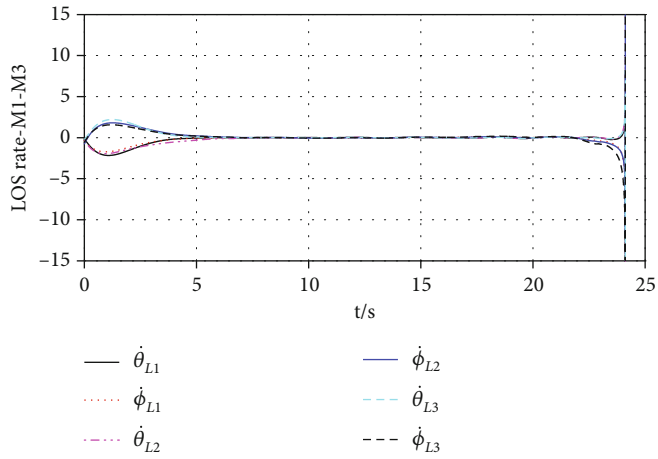

Figure 7: LOS angular rates under the proposed scheme.

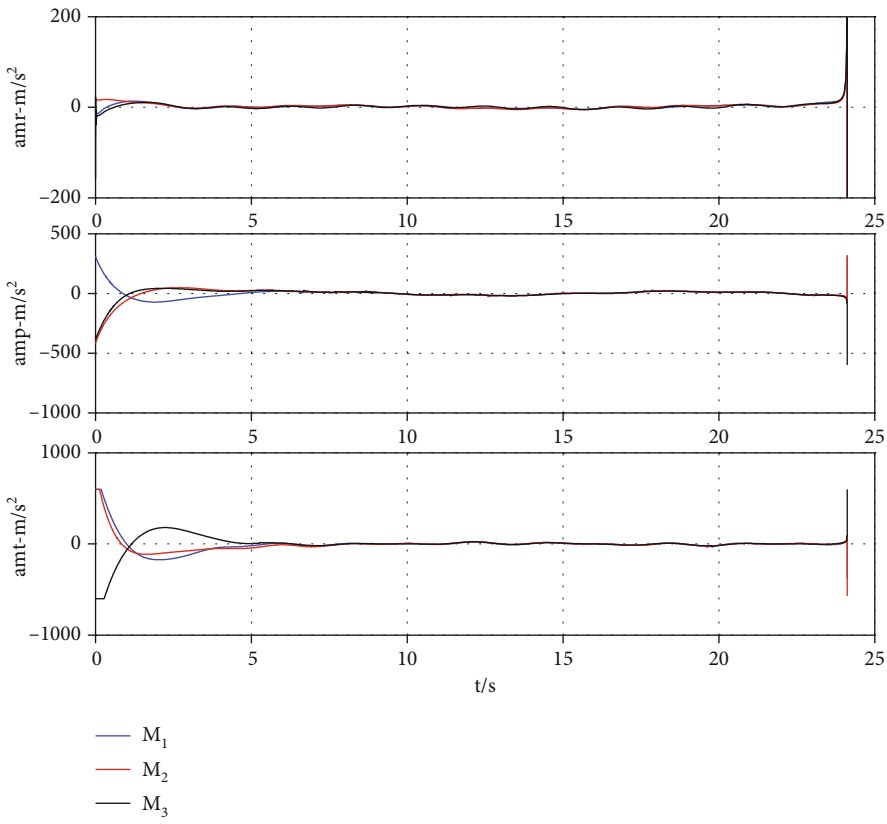

Figure 8: Acceleration commands under the proposed scheme.

By using Lemma 4, V_3 will converge to the following small region:

$$\Phi_{V_3} = \left\{ \left(s_{\phi i}, \kappa^*_{\phi i} - \hat{\kappa}^*_{\phi i} \right) | V_3 \le \min \left\{ \left(\frac{\bar{\Delta}_3}{\bar{k}_1 (1-\theta_q)} \right)^{2/1+\bar{p}_2}, \left(\frac{\bar{\Delta}_3}{\bar{k}_2 (1-\theta_q)} \right)^{2/1+\bar{q}_2} \right\}, (0 < \theta_q \le 1), \right. \tag{48}$$

within the fixed time $T_3 = 2/[\bar{k}_1(1-\bar{p}_2)] + 2/[\bar{k}_2(\bar{q}_2 - 1)]$, while fixed-time sliding mode variable (33) can be steered to the set

$$\Phi_{s_{\phi i}} = \left\{ s_{\phi i} \left| |s_{\phi i}| \le \sqrt{2} \min \left\{ \left(\frac{\bar{\Delta}_3}{\bar{k}_1 (1-\theta_q)} \right)^{1/1+\bar{p}_2}, \left(\frac{\bar{\Delta}_3}{\bar{k}_2 (1-\theta_q)} \right)^{1/1+\bar{q}_2} \right\} \right\}. \tag{49}$$

Since $s_{\phi i}$ is bounded after fixed-time convergence, it can be inferred that $|\dot{s}_{\phi i}| \le \delta_{\dot{s}_{\phi i}}$ holds with the constant $\delta_{\dot{s}_{\phi i}} > 0$. Then, it can be furthermore discussed about the neighbourhoods of the equilibrium point LOS angular rates and angle errors.

Table 2: Simulation results under different guidance laws.

Guidance law	M_i	Impact time (s)	Miss distance (m)	$\phi_{Li} - \phi_{Ld}$ (°)	$\theta_{Li} - \theta_{Ld}$ (°)
The proposed scheme	M_1	24.1240	0.0601	0.2133	0.0036
	M_2	24.1240	0.0627	0.2384	-0.0211
	M_3	24.1240	0.0634	0.2976	0.0068
Guidance law in [30]	M_1	24.1300	0.1428	0.6437	0.1420
	M_2	24.1190	0.1431	0.5980	0.0870
	M_3	24.1280	0.1460	0.6920	-0.7650
Guidance law in [15]	M_1	24.1900	0.2218	1.4225	1.3627
	M_2	24.1901	0.2109	1.4871	1.3657
	M_3	24.1900	0.2118	-1.3456	-1.2766
APN	M_1	23.8371	0.1792	2.3308	3.8237
	M_2	24.8946	0.3764	-8.3068	2.8637
	M_3	23.2901	0.3225	-7.3357	-7.9786

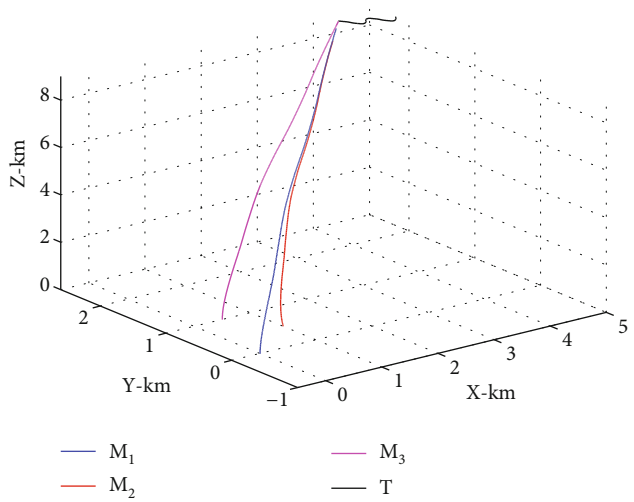

Figure 9: The trajectories of 3D engagement under APN guidance law.

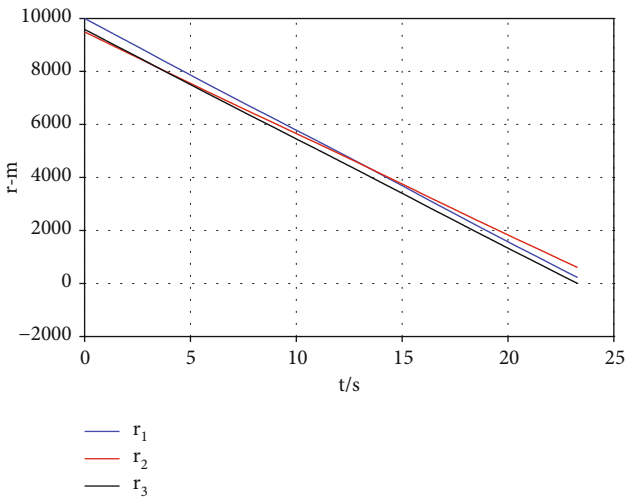

Figure 10: Relative distances under APN guidance law.

Therefore, from Theorem 16, it can be inferred that the closed-loop guidance subsystem is practical fixed-time stable.

Secondly, consider the subsystem for LOS angular rate and elevation angle

$$\begin{cases} \dot{x}_{5i} = x_{6i}, \\ \dot{x}_{6i} = -\dfrac{2x_{2i}x_{6i}}{x_{1i}} - x_{4i}\sin\theta_i\cos\theta_i - \dfrac{a_{M\theta i}}{x_{1i}} + d_{\theta i}. \end{cases} \tag{50}$$

From assumptions (i)-(iii), it can be inferred that the perturbations $d_{\theta i}$ are also bounded. Similarly, it can be supposed that there exist unknown scalars $\kappa_{\theta i} > 0$ such that $|d_{\theta i}| = |a_{T\theta i}/x_{1i}| \le \kappa_{\theta i}\Theta_{\theta i}$ is satisfied with $\Theta_{\theta i} = 1/x_{1i}$. Furthermore, fixed-time SM surface is constructed by

$$s_{\theta i} = x_{6i} + \iota_{21}x_{5i} + \iota_{22}g_{\theta i}(x_{5i}), \tag{51}$$

$$g_{\theta i}(x_{5i}) = \begin{cases} \dfrac{|x_{5i}|^{p'+1}}{\tanh x_{5i}}, \text{ if } \bar{s}_{\theta i} = 0 \| (\bar{s}_{\theta i} \neq 0 \&\& |x_{5i}| > \varepsilon_\theta), \\ k_{21}x_{5i} + k_{22}\mathrm{sig}^2(x_{5i}), \text{ else } \bar{s}_{\theta i} \neq 0 \&\& |x_{5i}| \le \varepsilon_\theta, \end{cases} \tag{52}$$

$$\bar{s}_{\theta i} = x_{6i} + \iota_{21}x_{5i} + \iota_{22}\frac{|x_{5i}|^{p'+1}}{\tanh x_{5i}}, \tag{53}$$

with $\iota_{21} > 0$, $\iota_{22} > 0$, $k_{21} = (1-p')\varepsilon_\theta^{p'}/\tanh\varepsilon_\theta$, $k_{22} = p'\varepsilon_\theta^{p'-1}/\tanh\varepsilon_\theta$, and small positive constant ε_θ. Then, fixed-time guidance law can be designed as

$$a_{M\theta i} = x_{1i}\cdot\left(a_{n\theta i} + k_{\theta 1}\mathrm{sig}^{\bar{p}_3}(s_{\theta i}) + k_{\theta 2}\mathrm{sig}^{\bar{q}_3}(s_{\theta i}) + \frac{\widehat{\kappa}_{\theta i}^{*}\Theta_{\theta i}^{*}s_{\theta i}}{2\mu_i^2}\right), \tag{54}$$

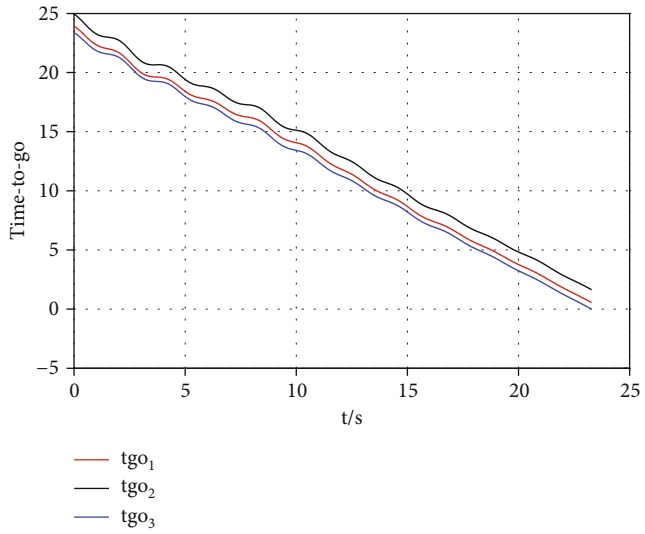

Figure 11: Time-to-go under APN guidance law.

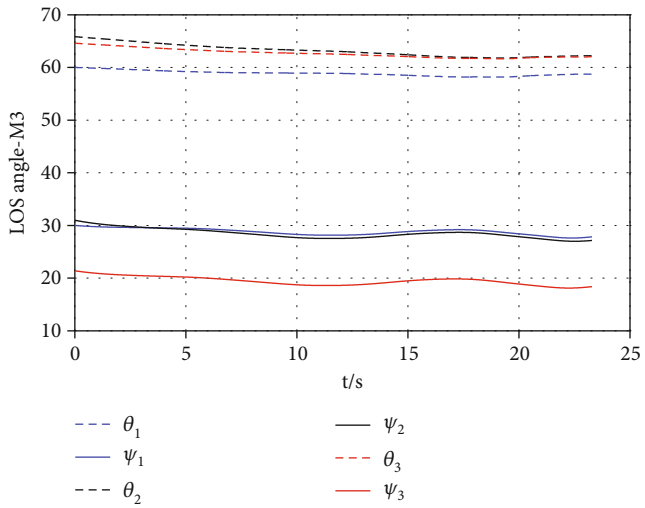

Figure 12: LOS angles under APN guidance law.

$$a_{n\theta i} = -\frac{2x_{2i}x_{6i}}{x_{1i}} - x_{4i}\sin\theta_i\cos\theta_i + \iota_{21}x_{6i} + \iota_{22}\dot{g}_{\theta i}(x_{5i}), \tag{55}$$

$$\dot{\widehat{\kappa}}^*_{\theta i} = \rho_{1i}\left(\frac{\Theta^*_{\theta i}s^2_{\theta i}}{2\mu_i^2} - \rho_{2i}\widehat{\kappa}^*_{\theta i}\right), \tag{56}$$

with the chosen positive constants $k_{\theta 1}$, $k_{\theta 2}$, ρ_{1i}, and ρ_{2i}. $\widehat{\kappa}^*_{\theta i}$ is the estimation of $\kappa^2_{\theta i}$; $\Theta^*_{\theta i}$ is implemented to denote $\Theta^2_{\theta i}$; the constant $\mu_i > 0$ is satisfied. □

Theorem 20. *Consider subsystem (50) with SM variable (51), and adaptive fixed-time guidance law (54)–(56) can steer LOS angular rates and angle errors to small regions around the origin within the fixed time.*

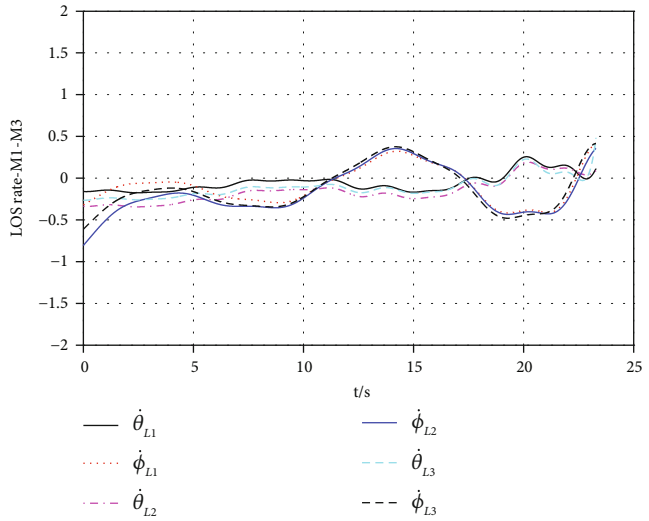

Figure 13: LOS rates under APN guidance law.

Proof. The relevant proof is similar to that of Theorem 18, which is omitted here. □

Remark 21. Adaptive laws are implemented to estimate the square of the upper bound for target acceleration. Due to nonexistent sign function, the chattering phenomenon is also properly solved. Consequently, the continuous control scheme can effectively improve the bombardment effect, only by relying on the information on the detected position and velocity of manoeuvring target.

Remark 22. Adaptive fixed-time consensus law and guidance law are in essence adaptive ISM and NTSM control algorithms, and therefore, fixed-time performance criterions are determined by the convergent time of sliding mode variables and system states. Moreover, the adaptive switch gains can reduce miss distance but then can also increase energy consumption. Therefore, these characteristics should be noticed in the process of the design of control laws and parameter selections.

Remark 23. When the designed fixed-time guidance law is applied to engagement geometry, the choice of guidance parameters can comply with the following procedure. Firstly, roughly evaluate the interception time between each missile and target on the basis of relative distance and velocity. Then, select control parameters to establish fixed-time consensus and guidance law and guarantee that the settling time of cooperative and guidance subsystem is kept within reasonable ranges. In addition, it is necessary to balance control energy consumption, miss distance, and settling time of closed-loop system. In terms of specific details, one standard procedure can be implemented by trial and error until the specified indicators are satisfactorily acquired for choosing these parameters.

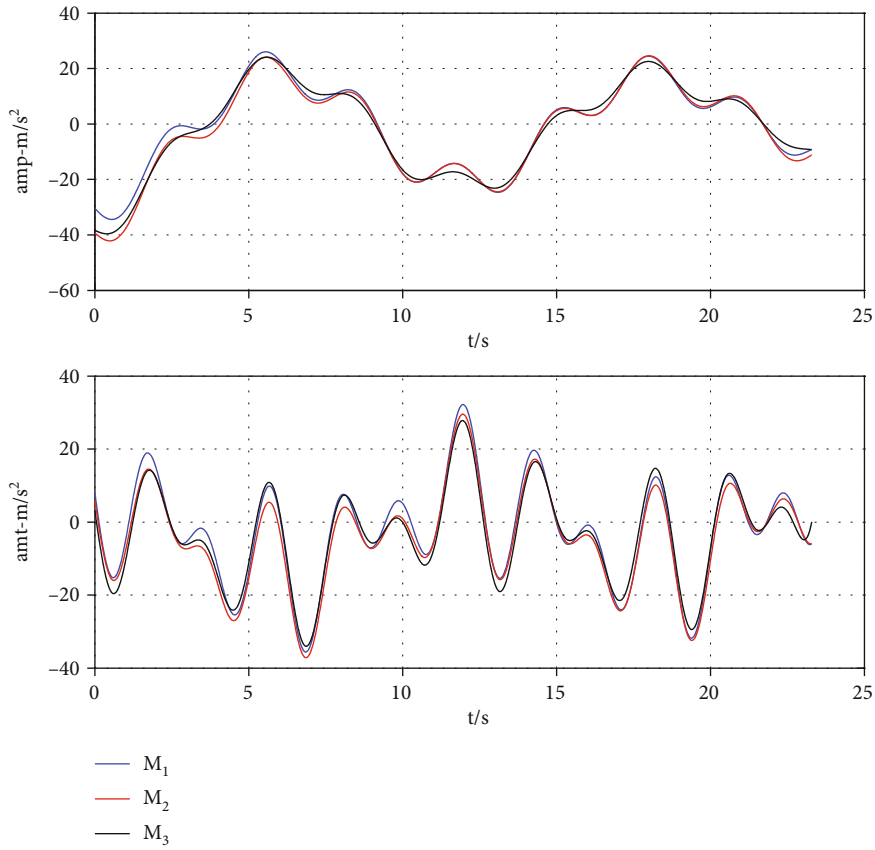

Figure 14: Acceleration commands under APN guidance law.

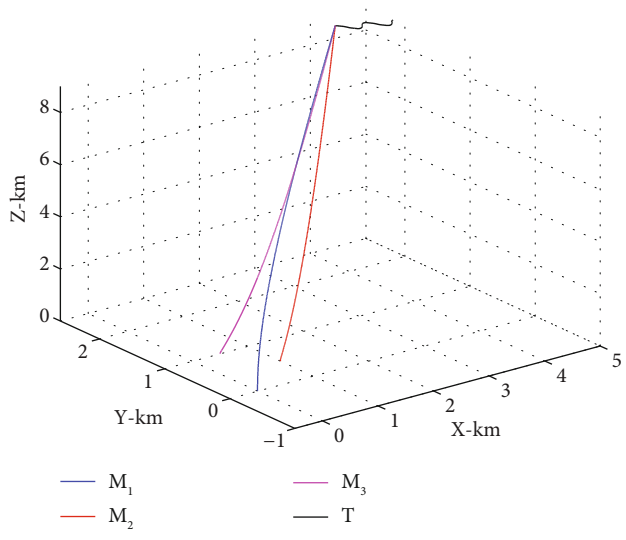

Figure 15: The trajectories of 3D engagement under cooperative guidance law [15].

4. Simulation Results and Discussion

To verify the guidance performance of the designed algorithm, numerical simulations are performed to show that three tactical missiles from different battle fields jointly intercept aerial manoeuvring target. Therein, the connected communication topology of three missiles is provided in Figure 2, and initial conditions are listed in Table 1. The relevant parameters of the proposed guidance law are selected as follows: $\alpha = \beta = \gamma = 0.2$, $p = 0.5$, $q = 1.2$, $\lambda_i = 1/2$, $\varepsilon_{ri} = 3/4$, $\bar{p}_1 = 0.8$, $\bar{q}_1 = 1.2$, $\eta_1 = 0.21$, $\eta_2 = 0.34$, $c_{0i} = 32$, $c_{1i} = 0.4$, $\iota_{11} = 0.4$, $\iota_{12} = 0.6$, $p' = 0.6$, $k_{\phi 1} = 0.32$, $k_{\phi 2} = 0.42$, $\varpi_i = 0.5$, $\gamma_{1i} = 12$, $\gamma_{2i} = 3$, $\bar{p}_2 = 0.8$, $\bar{q}_2 = 1.4$, $\iota_{21} = 0.4$, $\iota_{22} = 0.6$, $k_{\theta 1} = 0.32$, $k_{\theta 2} = 0.42$, $\mu_i = 0.5$, $\rho_{1i} = 12$, $\rho_{2i} = 3$, $\bar{p}_3 = 0.8$, and $\bar{q}_3 = 1.4$. The maximum accelerations along a_{Mri}, $a_{M\phi i}$, and $a_{M\theta i}$ are, respectively, limited to $40g$, $60g$, and $60g$, where g denotes gravitational acceleration. The initial positions of the missiles and target are (0, 0, 0), (1000, 500, 0), (500, 1000, 0), and $(2500\sqrt{3}, 2500, 5000\sqrt{3})$, respectively, while the initial velocity of incoming target is (20, -15, 18) m/s. The corresponding acceleration of the target is presumed as $a_{Tx} = 10 \sin(2t)\text{m}^2/\text{s}$, $a_{Ty} = -18 \cos(t/2)\text{m}^2/\text{s}$, and $a_{Tz} = -17 \sin(3t)\text{m}^2/\text{s}$, and target acceleration in other frames can be obtained by transformation matrix. In addition, comparison simulations are provided with augmented proportional guidance (APN), similar guidance law [15, 30] to test the merits of the proposed scheme.

The simulation results are provided in Figures 3–8. Three-dimensional engagement trajectories are described in Figure 3, while the relative distances are shown in Figure 4. Final miss distances and interception time are shown in Table 2 between each missile and manoeuvrable target. It can be seen that all the interceptors can effectively

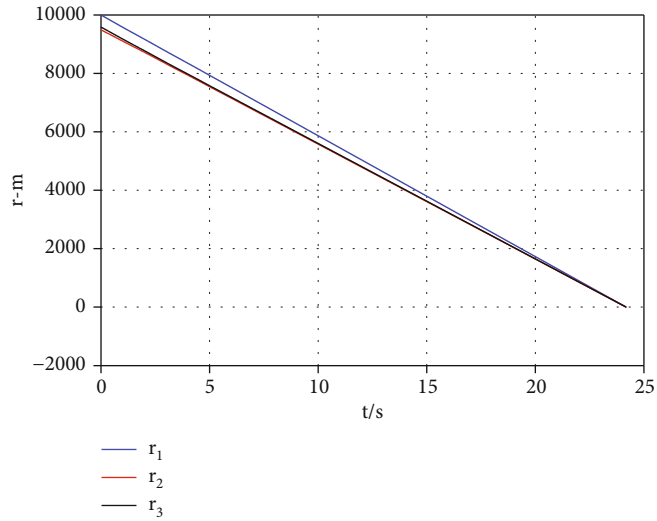

Figure 16: Relative distances under cooperative guidance law [15].

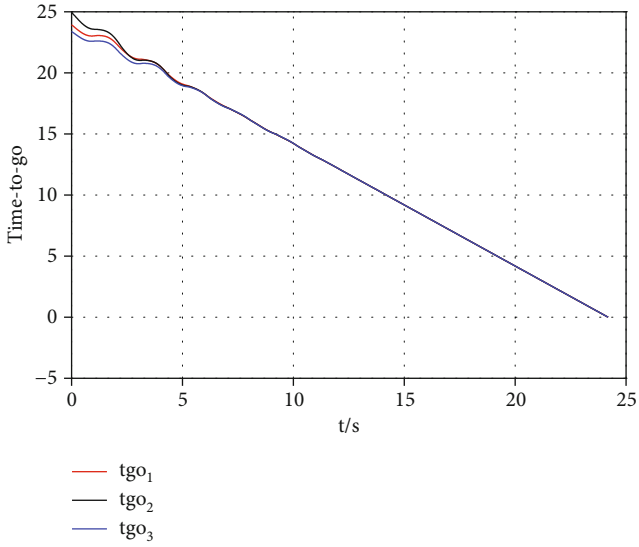

Figure 17: Time-to-go under cooperative guidance law [15].

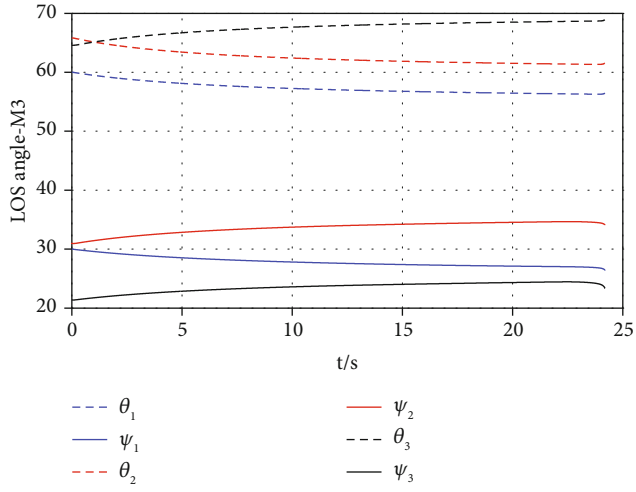

Figure 18: LOS angles under cooperative guidance law [15].

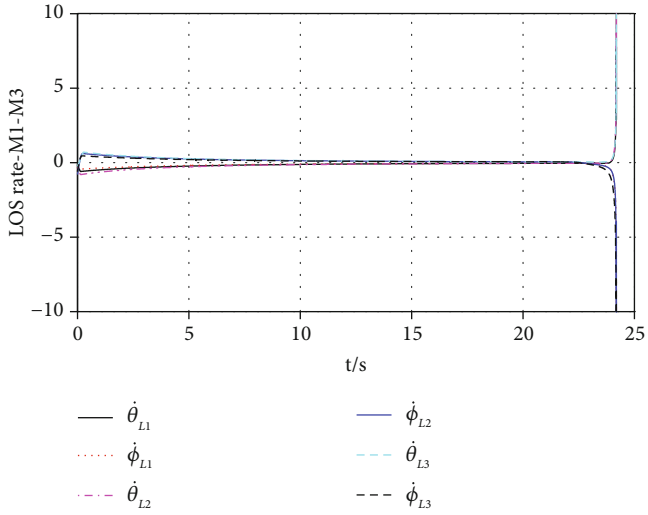

Figure 19: LOS rates under cooperative guidance law [15].

hit manoeuvring target. In addition, each missile adjusts its azimuth and elevation angles at the initial stage and ultimately strikes the incoming target at the desired impact angles.

The consensus of t_{goi} is achieved after 3.5 s, which is given in Figure 5, and fast fixed-time convergence can be guaranteed in the beginning. LOS angles and angular rates are depicted in Figures 6 and 7, respectively. It can be obtained that the LOS angles are forced to the desired values under the proposed algorithms, while fixed-time stabilization can also be achieved. Acceleration commands are exhibited in Figure 8. It can be seen that the initial values are relatively large since initial errors of time-to-go and LOS angle are large. After these errors converge to the neighbourhoods of the equilibrium point, acceleration commands become smaller and nearly sinusoidal due to target manoeuvre. From the above simulation results, it can be concluded that simultaneous arrival with the setting LOS angles is

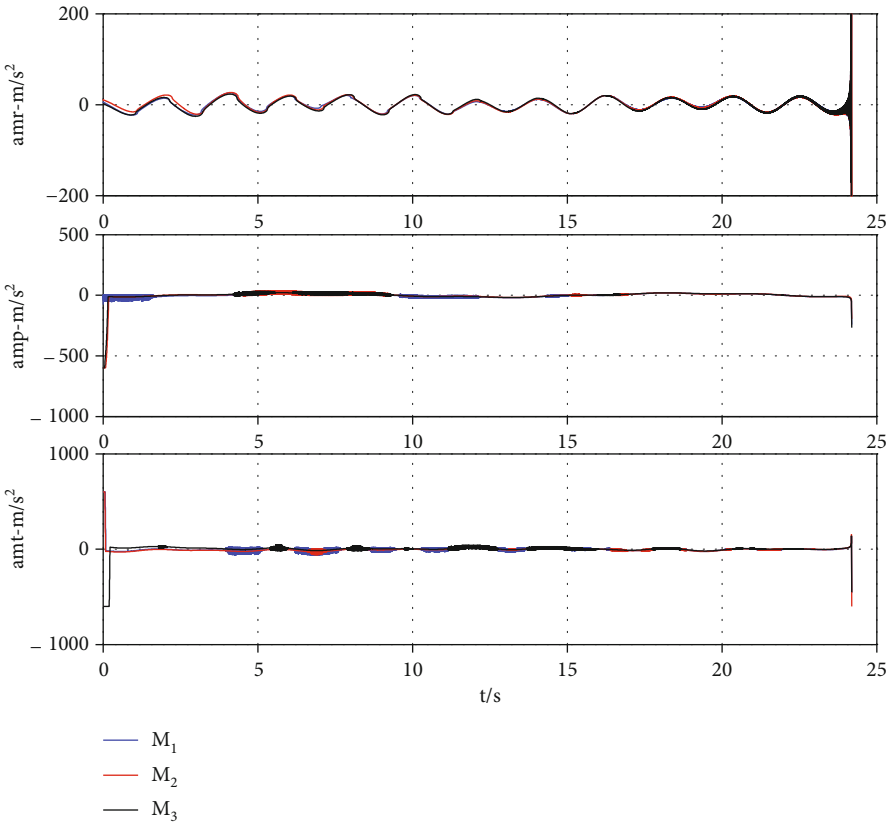

Figure 20: Acceleration commands under cooperative guidance law [15].

realized, and the performance of the proposed scheme is effectively validated.

To further demonstrate the effectiveness of the proposed scheme, the comparative simulations are provided for the conventional APN guidance law and similar guidance law [15]. The initial engagement conditions are the same as described in the previous paragraph. Therein, the APN guidance law is given as $a_{M\phi i} = -N\dot{r}_i\dot{\phi}_i + Na_{T\phi}/2$ and $a_{M\theta i} = -N\dot{r}_i\dot{\theta}_i + Na_{T\theta}/2$, where N is navigation ratio, which can be chosen as in the range of 3~5.

Simulation results of APN guidance law are provided in Figures 9–14. The motion trajectories are shown in Figure 9, and only the third missile hit the target. At the moment of the third missile collision with the target, from Figure 10, it can be seen that there are still some distances between the other missiles and the target. That is to say, simultaneous arrival is not realized. Due to the lack of consensus protocol, time-to-go cannot be steered to the same value in Figure 11. LOS angles and rates are provided in Figures 12 and 13, respectively, and it can be obtained that each missile can adjust its LOS angles and rates under APN guidance law, but the expected LOS angles can be kept to attack the target. Acceleration commands are depicted in Figure 14, and it can be obtained that guidance laws are always changing due to the target manoeuvring. Although APN guidance law does not play a role in simultaneous attack and impact angle constant, this law is concise and highly versatile.

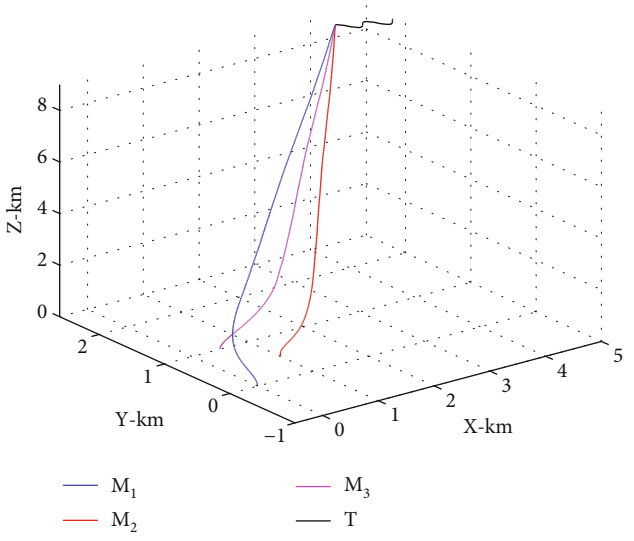

Figure 21: The trajectories of 3D engagement under cooperative guidance law [30].

Simulation results of similar cooperative guidance law [15] with adaptive law, ISM, and TSM are exhibited in Figures 15–20. From Figure 15, it can be observed that these missiles can intercept the manoeuvring target. The relative distances and time-to-go are shown in Figures 16 and 17, respectively. It can be obtained that simultaneous arrival

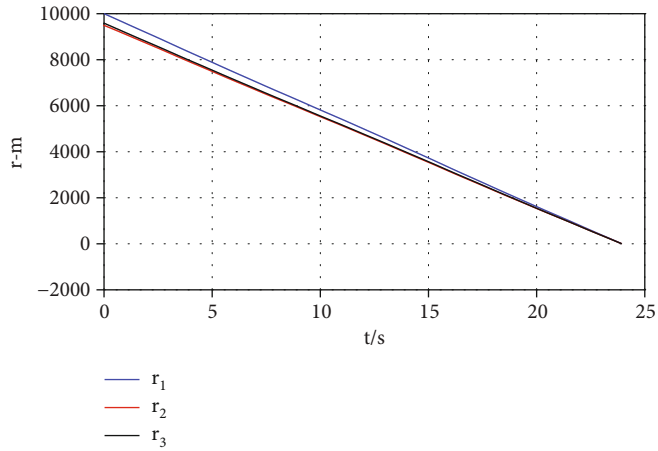

Figure 22: Relative distances under cooperative guidance law [30].

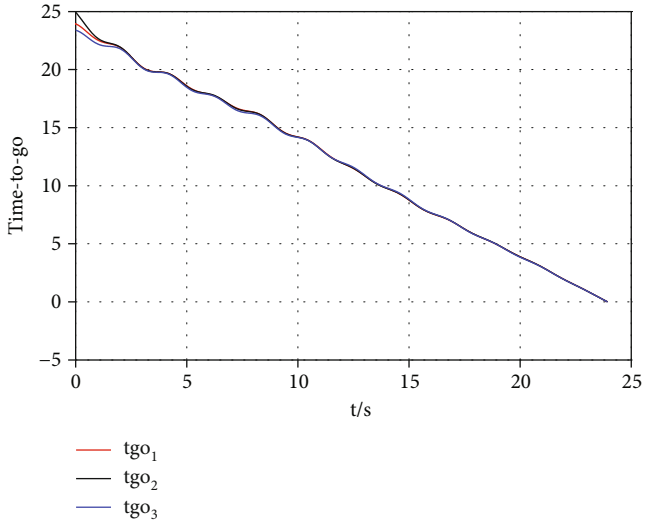

Figure 23: Time-to-go under cooperative guidance law [30].

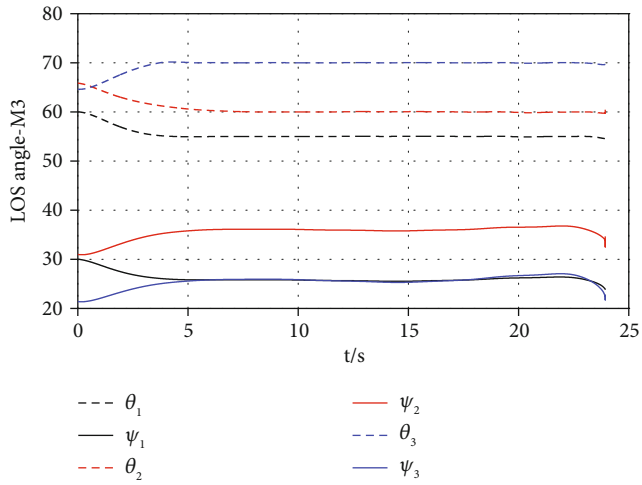

Figure 24: LOS angles under cooperative guidance law [30].

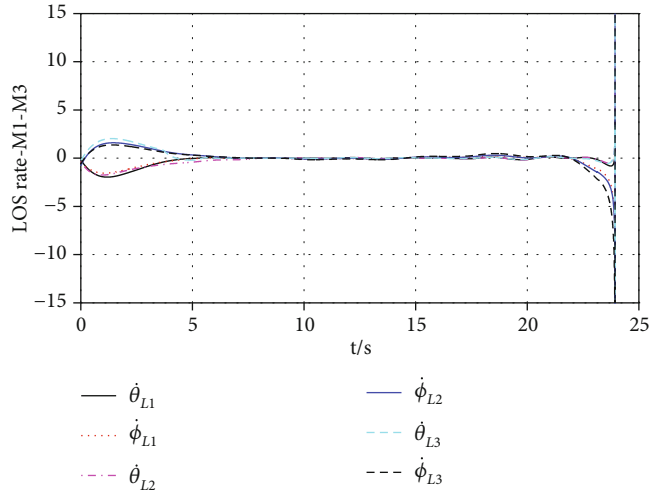

Figure 25: LOS rates under cooperative guidance law [30].

can be achieved, and miss distances are slightly larger but still more reasonable as shown in Table 2. In addition, time-to-go consensus is guaranteed, while the convergent time is longer than that of the proposed scheme compared with Figures 5 and 17. In elevation and azimuth directions, it can be obtained that LOS angles can be forced to the expected values in Figure 18, and LOS angular rates can converge the equilibrium points in Figure 19. Hence, the missiles are capable of hitting the target with the desired impact angles. However, the settling time of 14.2 s is longer that those of the proposed scheme. Acceleration commands are described in Figure 20, and it can be obtained that guidance law decreases to zero after LOS angle errors and angular rates converge to the origin. Due to the fact that the parameters of adaptive supertwist algorithm only increase without decreasing, the acceleration commands fluctuate continuously.

Simulation results of similar cooperative guidance law [30] with disturbance observer and TSM are exhibited in Figures 21–26. From Figure 21, it can be obtained that all the missiles can hit the manoeuvring target. The relative

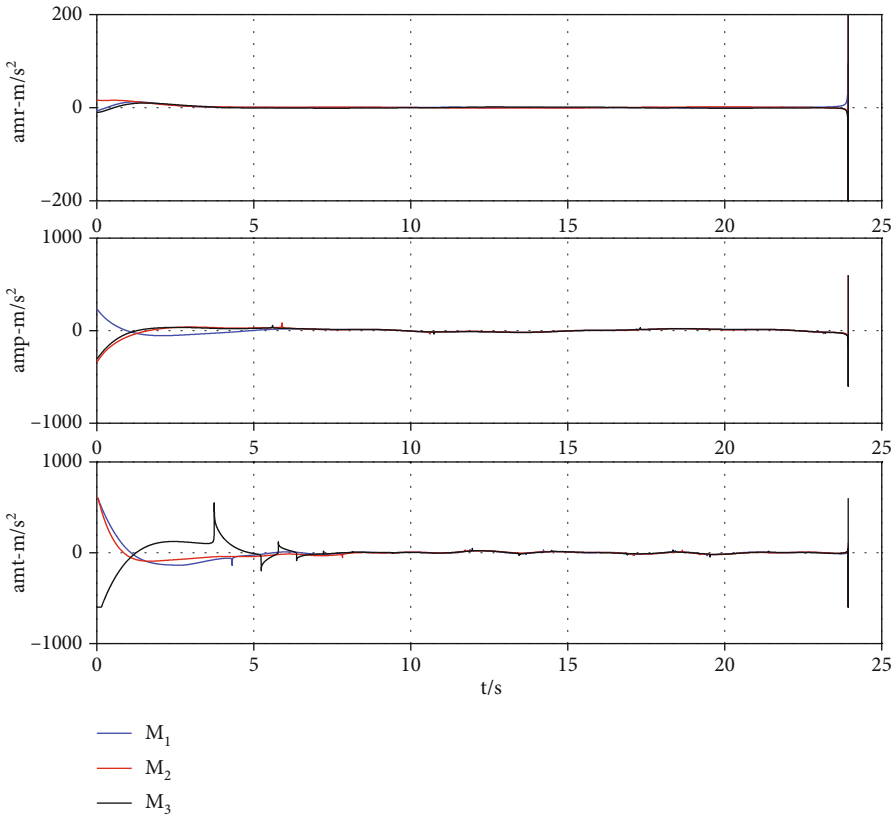

Figure 26: Acceleration commands under cooperative guidance law [30].

distances and time-to-go are described in Figures 22 and 23, respectively. It can be seen that time-to-go synchronization can be achieved, and miss distances are reasonable as shown in Table 2. In addition, time-to-go consensus is guaranteed, while the settling time is slightly longer than that of the proposed scheme as shown in Figures 5 and 23. In elevation and azimuth directions, it can be obtained that the expected LOS angles can be reached as shown in Figure 24, and LOS angular rates can converge the origin as shown in Figure 25. Hence, the missiles could intercept the target with the desired impact angles. However, the convergent time of 7.6 s is longer that those of the proposed scheme. Acceleration commands are shown in Figure 26, and it can be obtained that the change curves of the guidance law [30] are similar to those of the proposed algorithm. The cooperative guidance law is relatively concise, but low-pass filters and disturbance observer have certain impact on the interception time and guidance accuracy.

5. Conclusions

In this paper, distributed 3D fixed-time cooperative guidance scheme has been presented to accomplish salvo attack at the desired impact angles. The average value of time-to-go is achieved through information interaction in fixed time, and therefore, the bombardment is finally completed at the same time. In the azimuth and elevation direction of the LOS, novel adaptive fixed-time guidance commands are proposed to guarantee that LOS angular rates are driven to the neighbourhood of the origin in the specified time. The whole guidance process only needs the information from adjacent missiles and the position and speed of an incoming target. In the future, more constraints or realistic environments will be considered in the cooperative attack of multiple missiles against manoeuvring target.

Data Availability

The data that support the findings of this study are available from the authors.

Conflicts of Interest

The authors declare that there is no conflict of interest regarding the publication of this paper.

Acknowledgments

This work was supported in part by the Aeronautical Science Foundation of China under Grant 20180142001.

References

[1] X. Wang, Y. Zhang, and H. Wu, "Distributed cooperative guidance of multiple anti-ship missiles with arbitrary impact angle constraint," *Aerospace Science and Technology*, vol. 46, pp. 299–311, 2015.

[2] C. Wang, W. Dong, J. Wang, and M. Xin, "Impact-angle-constrained cooperative guidance for salvo attack," *Journal of*

Guidance, Control, and Dynamics, vol. 45, no. 4, pp. 684–703, 2022.

[3] W. Dong, F. Deng, C. Wang, J. Wang, and M. Xin, "Three-dimensional spatial-temporal cooperative guidance without active speed control," *Journal of Guidance, Control, and Dynamics*, vol. 46, no. 10, pp. 1981–1996, 2023.

[4] X. Wang and C. Tan, "3-D impact angle constrained distributed cooperative guidance for maneuvering targets without angular-rate measurements," *Control Engineering Practice*, vol. 78, pp. 142–159, 2018.

[5] X. H. Wang and C. P. Tan, "Distributed cooperative controller design considering guidance loop and impact angle," *Journal of the Franklin Institute*, vol. 355, no. 15, pp. 6927–6946, 2018.

[6] X. Wang and X. Lu, "Three-dimensional impact angle constrained distributed guidance law design for cooperative attacks," *ISA Transactions*, vol. 73, pp. 79–90, 2018.

[7] I. S. Jeon, J. I. Lee, and M. J. Tahk, "Impact-time-control guidance law for anti-ship missiles," *IEEE Transactions on Control Systems Technology*, vol. 14, no. 2, pp. 260–266, 2006.

[8] C. Wang, X. Ding, J. Wang, and J. Shan, "A robust three-dimensional cooperative guidance law against maneuvering target," *Journal of the Franklin Institute*, vol. 357, no. 10, pp. 5735–5752, 2020.

[9] Z. Chen, J. Yu, X. Dong, and Z. Ren, "Three-dimensional cooperative guidance strategy and guidance law for intercepting highly maneuvering target," *Chinese Journal of Aeronautics*, vol. 34, no. 5, pp. 485–495, 2021.

[10] Y. Zhang, S. Tang, and J. Guo, "Two-stage cooperative guidance strategy using a prescribed-time optimal consensus method," *Aerospace Science and Technology*, vol. 100, article 105641, 2020.

[11] X. Ai, L. Wang, J. Yu, and Y. Shen, "Field-of-view constrained two-stage guidance law design for three-dimensional salvo attack of multiple missiles via an optimal control approach," *Aerospace Science and Technology*, vol. 85, pp. 334–346, 2019.

[12] D. Cho, H. J. Kim, and M. J. Tahk, "Nonsingular sliding mode guidance for impact time control," *Journal of Guidance, Control, Dynamics*, vol. 39, no. 1, pp. 61–68, 2016.

[13] Y. Zhao, Y. Sheng, and X. Liu, "Analytical impact time and angle guidance via time-varying sliding mode technique," *ISA Transactions*, vol. 62, pp. 164–176, 2016.

[14] G. Li, Y. Wu, and P. Xu, "Adaptive fault-tolerant cooperative guidance law for simultaneous arrival," *Aerospace Science and Technology*, vol. 82-83, pp. 243–251, 2018.

[15] J. Song, S. Song, and S. Xu, "Three-dimensional cooperative guidance law for multiple missiles with finite-time convergence," *Aerospace Science and Technology*, vol. 67, pp. 193–205, 2017.

[16] E. Zhao, T. Chao, S. Wang, and M. Yang, "Multiple flight vehicles cooperative guidance law based on extended state observer and finite time consensus theory," *Proceeding of the Institution of Mechanical Engineers Part G Journal of Aerospace Engineering*, vol. 232, no. 2, pp. 270–279, 2018.

[17] S. Zhang, Y. Guo, Z. Liu, S. Wang, and X. Hu, "Finite-time cooperative guidance strategy for impact angle and time control," *IEEE Transactions on Aerospace and Electronic Systems*, vol. 57, no. 2, pp. 806–819, 2021.

[18] T. Lyu, C. Li, Y. Guo, and G. Ma, "Three-dimensional finite-time cooperative guidance for multiple missiles without radial velocity measurements," *Chinese Journal of Aeronautics*, vol. 32, no. 5, pp. 1294–1304, 2019.

[19] J. Gao and Y. L. Cai, "Three-dimensional impact angle constrained guidance laws with fixed-time convergence," *Asian Journal of Control*, vol. 19, no. 6, pp. 2240–2254, 2017.

[20] G. Li, Y. Wu, and P. Xu, "Fixed-time cooperative guidance law with input delay for simultaneous arrival," *International Journal of Control*, vol. 94, no. 6, pp. 1664–1673, 2021.

[21] M. Lin, X. Ding, C. Wang, L. Liang, and J. Wang, "Three-dimensional fixed-time cooperative guidance law with impact angle constraint and prespecified impact time," *IEEE Access*, vol. 9, pp. 29755–29763, 2021.

[22] W. Dong, C. Wang, J. Wang, Z. Zuo, and J. Shan, "Fixed-time terminal angle-constrained cooperative guidance law against maneuvering target," *IEEE Transactions on Aerospace and Electronic Systems*, vol. 58, no. 2, pp. 1352–1366, 2022.

[23] H. Hu, K. Dai, H. Li et al., "Three-dimensional adaptive fixed-time cooperative guidance law with impact time and angle constraints," *Aerospace Science and Technology*, vol. 123, article 107450, 2022.

[24] X. Li, J. Ma, J. Gao, and S. Zang, "Adaptive super-twisting cooperative guidance law with fixed-time convergence," *International Journal of Aerospace Engineering*, vol. 2022, Article ID 8650592, 17 pages, 2022.

[25] Z. Chen, W. Chen, X. Liu, and J. Cheng, "Three-dimensional fixed-time robust cooperative guidance law for simultaneous attack with impact angle constraint," *Aerospace Science and Technology*, vol. 110, article 106523, 2021.

[26] P. Zhang and X. Y. Zhang, "Multiple missiles fixed-time cooperative guidance without measuring radial velocity for maneuvering targets interception," *ISA Transactions*, vol. 126, pp. 388–397, 2022.

[27] D. Zhou, S. Sun, and K. L. Teo, "Guidance laws with finite time convergence," *Journal of Guidance, Control, and Dynamics*, vol. 32, no. 6, pp. 1838–1846, 2009.

[28] H.-S. Shin, A. Tsourdos, and K. B. Li, "A new three-dimensional sliding mode guidance law variation with finite time convergence," *IEEE Transactions on Aerospace and Electronic Systems*, vol. 53, no. 5, pp. 2221–2232, 2017.

[29] J. P. Mishra, C. Li, M. Jalili, and X. Yu, "Robust second-order consensus using a fixed-time convergent sliding surface in multiagent systems," *IEEE Transactions on Cybernetics*, vol. 50, no. 2, pp. 846–855, 2020.

[30] H. X. Li, H. J. Li, and Y. L. Cai, "Three-dimensional cooperative guidance law to control impact time and angle with fixed-time convergence," *Proceedings of the Institution of Mechanical Engineers, Part G, Journal of Aerospace Engineering*, vol. 236, no. 8, pp. 1647–1666, 2022.

[31] B. Tian, H. Lu, Z. Zou, and W. Yang, "Fixed-time leader-follower output feedback consensus for second-order multiagent systems," *IEEE Transactions on Cybernetics*, vol. 49, no. 4, pp. 1545–1550, 2019.

[32] Y. Xu, Z. Yao, R. Lu, and B. Ghosh, "A novel fixed-time protocol for first-order consensus tracking with disturbance rejection," *IEEE Transactions on Automatic Control*, vol. 67, no. 11, pp. 6180–6186, 2022.

[33] V. T. Haimo, "Finite-time controllers," *SIAM Journal on Control and Optimization*, vol. 24, no. 4, pp. 760–770, 1986.

[34] S. P. Bhat and D. S. Bernstein, "Continuous finite-time stabilization of the translational and rotational double integrators," *IEEE Transactions on Automatic Control*, vol. 43, no. 5, pp. 678–682, 1998.

[35] A. Polyakov, "Nonlinear feedback design for fixed-time stabilization of linear control systems," *IEEE Transactions on Automatic Control*, vol. 57, no. 8, pp. 2106–2110, 2012.

[36] Z. Zuo and L. Tie, "A new class of finite-time nonlinear consensus protocols for multi-agent systems," *International Journal of Control*, vol. 87, no. 2, pp. 363–370, 2014.

[37] J. Gao, Z. Fu, and S. Zhang, "Adaptive fixed-time attitude tracking control for rigid spacecraft with actuator faults," *IEEE Transactions on Industrial Electronics*, vol. 66, no. 9, pp. 7141–7149, 2019.

[38] W. Chen, M. Liu, and Q. Hu, "Attitude tracking control for spacecraft with fixed-time convergence," *IFAC-PapersOnLine*, vol. 53, no. 2, pp. 14857–14862, 2020.

[39] R. Olfati-Saber and R. M. Murray, "Consensus problems in networks of agents with switching topology and time-delays," *IEEE Transactions on Automatic Control*, vol. 49, no. 9, pp. 1520–1533, 2004.